UNIVERSITAT POLITÈCNICA DE CATALUNYA
BARCELONATECH
Escola d'Enginyeria de Barcelona Est

TREBALL FI DE GRAU

Grau en Enginyeria de l'Energia

OPTIMAL POWER FLOW FOR HYBRID AC/DC GRIDS

Memòria i Annexos

Autor: Quim Espadalé Bonet
Director: Raúl Benítez Iglesias
Co-Director: Xiong Xiao M.Sc. (TU Darmstadt)

Convocatòria: Gener 2022

Optimal Power Flow for Hybrid AC/DC Grids

Bachelor Thesis

Quim Espadalé Bonet | Bachelor's Degree in Energy Engineering

Electrical Power Supply with Integration of Renewable Energy

Prof. Dr.-Ing. Jutta Hanson

TECHNISCHE UNIVERSITÄT DARMSTADT

Elektrische Energieversorgung unter Einsatz Erneuerbarer Energien

Institute for Electrical Energy Systems

Electrical Power Supply with Integration of Renewable Energy
Prof. Dr.-Ing. Jutta Hanson

TECHNISCHE UNIVERSITÄT DARMSTADT

Elektrische Energieversorgung unter Einsatz Erneuerbarer Energien

Darmstadt, 28.01.2022

Thesis Nr. B-790

by

Quim Espadalé Bonet

Optimal Power Flow for Hybrid AC/DC Grids

In this thesis, an OPF calculation model applied to AC/DC hybrid grids is presented, with the aim of developing an extension of MatPower that allows this type of calculation. With this tool, it is carried out the study of the OPF for a test system defined by a hybrid grid.

Ausgabetermin:	06.09.2021
Einlieferungstermin:	28.01.2022
Betreuung:	Xiong Xiao M.Sc., Soham Choudhury M.Sc.

Prof. Dr.-Ing. Jutta Hanson

Quim Espadalé Bonet
Matriculation Number: 2498364
Field of studies: Energy Engineering (UPC – Universitat Politècnica de Catalunya)

Bachelor Thesis
Topic: Optimal Power Flow for Hybrid AC/DC Grids

Submitted: 28.01.2022

Supervision: Xiong Xiao M.Sc., Soham Choudhury M.Sc.

Prof. Dr.-Ing. Jutta Hanson
Fachgebiet Elektrische Energieversorgung unter Einsatz Erneuerbarer Energien
Technische Universität Darmstadt
Landgraf-Georg-Straße 4
64283 Darmstadt

Erklärung zur Abschlussarbeit

Hiermit versichere ich, Quim Espadalé Bonet, die vorliegende Abschlussarbeit gemäß § 22 Abs. 7 APB der TU Darmstadt ohne Hilfe Dritter und nur mit den angegebenen Quellen und Hilfsmitteln angefertigt zu haben. Alle Stellen, die Quellen entnommen wurden, sind als solche kenntlich gemacht worden. Diese Arbeit hat in gleicher oder ähnlicher Form noch keiner Prüfungsbehörde vorgelegen.

Mir ist bekannt, dass im Falle eines Plagiats (§38 Abs.2 APB) ein Täuschungsversuch vorliegt, der dazu führt, dass die Arbeit mit 5,0 bewertet und damit ein Prüfungsversuch verbraucht wird. Abschlussarbeiten dürfen nur einmal wiederholt werden.

Bei der abgegebenen Abschlussarbeit stimmen die schriftliche und die zur Archivierung eingereichte elektronische Fassung gemäß § 23 Abs. 7 APB überein.

Darmstadt, 28.01.2022

Quim Espadalé Bonet

Abstract

In this thesis, an OPF calculation model applied to AC/DC hybrid grids is presented, with the aim of developing an extension of MatPower that allows this type of calculation. With this tool, the OPF is studied for a test system defined by a hybrid grid.

First, an introduction to HVDC transmission systems is given. After this, the modelling of hybrid AC/DC grids is developed, adding converters and HVDC lines to the model for AC. Then, the OPF mathematical model is defined, whose objective function, variables and constraints associated with the hybrid AC/DC model are presented. From here, the test system to be studied is introduced and results are shown from the developed MatPower extension. These results allow comparing different scenarios for the test system, each one having an HVDC system with different levels of meshing.

Acknowledgements

I would first like to thank my supervisors, Xiong Xiao and Soham Choudhury, for all the dedication and hours of work shared. Without your help and feedback this thesis would not have been possible.

I would also like to thank Júlia for all the strength she has given me and for being there whenever I have needed her. And to my parents, who have been listening to me from home and encouraging me to take advantage of the experience.

I do not forget my friends Joan, Vicenç and Lluc, for the path we have traveled together to become engineers.

And I would especially like to thank Alberto, Diego, Davide, Achille, Anna, Giada, Walter, Gimmy and Carlos for all the moments we shared during the six months in Darmstadt. I come back home knowing that I have friends all over Europe.

Contents

List of figures

List of tables

Nomenclature

Abbreviations

AC	Alternating Current
DC	Direct Current
HVAC	High Voltage Alternating Current
HVDC	High Voltage Direct Current
ICC	Inner-Current Control
IGBT	Insulated-Gate Bipolar Transistor
LCC	Line Commutated Converter
MIPS	MatPower Interior Point Solver
MMC	Modular Multi-level Converter
MTDC	Multi-Terminal Direct Current
OHL	Over-Head Line
OPF	Optimal Power Flow
PDCI	Pacific Direct Current Intertie
PCC	Point of Common Coupling
PF	Power Flow
PLL	Phase-Locked Loop
PWM	Pulse Width Modulation
VSC	Voltage Source Converter

Nomenclature

a_i	No-load loss factor of the converter connected to AC node i
b_i	Linear current factor of the converter connected to AC node i
$B_{q,ij}$	Shunt susceptance for the AC line between nodes i and j
$B_{\mathrm{busAC},ij}$	Equivalent susceptance in the AC line between nodes i and j
$B_{\mathrm{f},i}$	AC low pass filter equivalent susceptance
$B_{\mathrm{t},i}$	Equivalent susceptance of the transformer of the converter station
$B_{\mathrm{c},i}$	Equivalent susceptance of the phase reactor of the converter station
$B_{\mathrm{tc},i}$	Equivalent susceptance of the transformer – phase reactor set
c_i	Square current factor of the converter connected to AC node i
$C_{\mathrm{G},i}$	Binary operation variable for the generators in the AC node i
$C_{\mathrm{S},i}$	Binary operation variable for the converters in the AC node i
C'	Equivalent capacitance of the cables in μF/km
$G_{\mathrm{q},ij}$	Shunt conductance for the AC line between nodes i and j

$G_{\mathrm{busAC},ij}$	Equivalent conductance in the AC line between nodes i and j
$G_{\mathrm{t},i}$	Equivalent conductance of the transformer of the converter station
$G_{\mathrm{c},i}$	Equivalent conductance of the phase reactor of the converter station
$G_{\mathrm{tc},i}$	Equivalent conductance of the transformer – phase reactor set
G^{S}	Equality constraint for the AC nodal power balance
G_{X}^{S}	First derivative for the AC nodal power balance constraint with respect to X
G_{XX}^{S}	Second derivative for the AC nodal power balance constraint with respect to XX
$G^{P_{\mathrm{dc}}}$	Equality constraint for the DC power flow
$G_{X}^{P_{\mathrm{dc}}}$	First derivative for the DC power flow constraint with respect to X
$G_{XX}^{P_{\mathrm{dc}}}$	Second derivative for the DC power flow constraint with respect to XX
G^{Conv}	Equality constraint for the converter losses
$G^{S_{\mathrm{c}}}$	Equality constraint for the converter AC PF (complex power)
$G^{P_{\mathrm{c}}}$	Equality constraint for the converter AC PF (active power)
$G^{Q_{\mathrm{c}}}$	Equality constraint for the converter AC PF (reactive power)
$G_{X}^{S_{\mathrm{c}}}$	First derivative for the converter AC PF constraint with respect to X
$G_{XX}^{S_{\mathrm{c}}}$	Second derivative for the converter AC PF constraint with respect to XX
G^{Active}	Equality constraint for the active channel of the control system
G^{Reactive}	Equality constraint for the reactive channel of the control system
$H^{\mathrm{I_c}}$	Inequality constraint for the current limits in the AC side of the converter
$H^{\mathrm{I_{dc}}}$	Inequality constraint for the current limits in the DC system
$I_{\mathrm{dc},i}$	Current flowing from the node i to the DC system
$I_{\mathrm{c},i}$	Current flowing in the AC side of the converter connected to AC node i
$I_{\mathrm{dc}}^{\max}$	Maximum value for the current flowing in the DC system
$I_{\mathrm{c}}^{\max}$	Maximum value for the current flowing in the AC side of the converter
i_{d}	Control current in the d-axis
i_{q}	Control current in the q-axis
k	Current iteration in the calculation process
m	Number of rows for a matrix
n	Number of columns for a matrix
$\mathrm{N_{ac}}$	Number on AC nodes in the studied system
P_{i}	Injected active power in the AC node i
$P_{\mathrm{G},i}$	Active power injected by the synchronous generators in the AC node i
$P_{\mathrm{L},i}$	Active power demanded by the load in the AC node i
$P_{\sum \mathrm{br},i}$	Active power injected to the AC transmission lines from the node i
$P_{\mathrm{s},i}$	Active power injected by the converter in the AC node i
$P_{\mathrm{dc},i}$	Power injected to the DC system from the converter connected to AC node i
$P_{\mathrm{loss},i}$	Power losses in the converter connected to AC node i
$P_{\mathrm{c},i}$	Active power in the AC side of the converter connected to AC node i

$P_{s,i}^{Ref}$	Reference value for the active injected power from the converter to node i
$P_{control}$	Control active power in the control system in the converter
$P_{dc,base}$	Base value for the DC power
Q_i	Injected reactive power in the AC node i
$Q_{G,i}$	Reactive power injected by the synchronous generators in the AC node i
$Q_{L,i}$	Reactive power demanded by the load in the AC node i
$Q_{\sum br,i}$	Reactive power injected to the AC transmission lines from the node i
$Q_{s,i}$	Reactive power injected by the converter in the AC node i
$Q_{c,i}$	Reactive power in the AC side of the converter connected to AC node i
$Q_{f,i}$	Reactive power absorbed by the filter of the converter station
$Q_{s,i}^{Ref}$	Reference value for the reactive injected power from the converter to node i
$Q_{control}$	Control reactive power in the control system in the converter
$R_{L,ij}$	Resistive component for the AC line impedance between nodes i and j
$R_{dc,ij}$	Equivalent resistance in the DC branch between nodes i and j
$R_{c,i}$	Resistive component of the phase reactor equivalent impedance
R'	Equivalent resistance of the cables in Ω/km
$R_{dc,base}$	Base value for the equivalent resistance of the DC branches
S_i	Injected complex or apparent power in the AC node i
$S_{c,i}$	Complex power in the AC side of the converter
$S_{s,i}$	Complex power injected to the AC system from the converter
$S_{cf,i}$	Complex power at the output of the phase reactor
$S_{sf,i}$	Complex power at the transformer input
S_i^{bus}	Complex mismatch power in the AC node i
$S_{L,i}$	Complex power demanded by the load in the AC node i
$S_{G,i}$	Complex power injected by the synchronous generators in the AC node i
$S_{s,i}$	Complex power injected by the converter in the AC node i
U_i	Voltage magnitude in the AC node i
$U_{dc,i}$	DC voltage in the DC node i
$U_{s,i}$	Injection voltage magnitude from the converter to the AC node i
$U_{c,i}$	Voltage magnitude in the AC side of the converter connected to node i
$U_{f,i}$	Voltage magnitude in the filter of the converter station
$U_{dc,i}^{Ref}$	Reference value for the DC voltage in the DC node i
$U_{s,i}^{Ref}$	Reference value for the injection voltage magnitude from the converter to node i
$U_{dc,base}$	Base value for the DC voltage
v_d	Control voltage in the d-axis
v_q	Control voltage in the q-axis
$X_{L,ij}$	Inductive component for the AC line impedance between nodes i and j
$X_{c,i}$	Inductive component of the phase reactor equivalent impedance

X'	Equivalent inductance of the cables in Ω/km
X	Any of the state variables on which the constraint depends
X_i^{Max}	Maximum value for any of the state variables
X_i^{Min}	Minimum value for any of the state variables
x^{T}	Optimization variables' vector
$Y_{\mathrm{q},ij}$	Shunt admittance for the AC line between nodes i and j
$\mathrm{Y}_{\mathrm{busAC}}$	Admittance matrix for the AC system
$y_{\mathrm{busAC},ij}$	Equivalent admittance in the AC line between nodes i and j
$y_{\mathrm{dc},ij}$	Equivalent admittance in the DC branch between nodes i and j
$\mathrm{Y}_{\mathrm{busDC}}$	Admittance matrix for the DC system
$y_{\mathrm{busDC},ij}$	Element of the DC system admittance matrix in the position ij
$Z_{\mathrm{L},ij}$	AC line impedance between nodes i and j
$Z_{\mathrm{c},i}$	Phase reactor equivalent impedance in the converter station
$Z_{\mathrm{t},i}$	Equivalent impedance of the transformer of the converter station
$Z_{\mathrm{tc},i}$	Equivalent impedance of the transformer – phase reactor set
θ_i	Voltage angle in the AC node i
$\theta_{\mathrm{s},i}$	Injection voltage angle from the converter to the AC node i
$\theta_{\mathrm{c},i}$	Voltage angle in the AC side of the converter connected to node i
$\theta_{\mathrm{f},i}$	Voltage angle in the filter of the converter station
λ	Lagrangian multiplier for equality constraints
μ	Lagrangian multiplier for inequality constraints

1 Introduction

1.1 Background

Around the world there is a clear concern about the environmental footprint that the human species is leaving over the years. The European Union, for example, has developed a series of objectives for all its member states based on three fundamental pillars: reduction in emissions, improvement in energy efficiency and increase in energy consumption from renewable sources [1]. Despite the improvement in global energy efficiency, an increase in consumption is expected in Europe over the coming decades [2]. This fact, added to a greater penetration of renewable energies in electrical power systems, supposes a technical challenge for the adaptation of the networks to these conditions.

If the electrical power systems of each country want to adapt to the new reality, they will have to implement a series of improvements that allow them to offer higher capacity, higher flexibility and better interconnectivity with the electrical power systems of neighbour countries. The variability of renewable energy resources makes necessary to have more interconnectivity between countries, since the energy deficits of one system could be supplied by the surpluses of another. This fact entails, together with the increase in consumption, the need for higher transmission capacity and more flexibility.

Adding HVDC transmission lines in the current electrical power systems can lead to an increase in the transmission capacity, taking in account the technological improvement around the cabling materials or the optimal use of the resources through the use of dynamic line rating. There is also the possibility of increasing the capacity of the system by replacing old HVAC lines with new HVDC lines, which implies an increase in the capacity of between 200% and 350% [2]. The HVDC lines allow an interconnection between distant or asynchronous systems in an efficient way maintaining a power flow between them. In addition, HVDC transmission is also optimal for the connection of remote generation systems, such as offshore wind farms, to the onshore electrical network.

For all these reasons, there are many countries that are already contemplating the installation of HVDC transmission to their electrical power systems, betting on a model based on hybrid AC/DC grids. And not only through point-to-point connections, but also by developing HVDC meshed systems and transmission sub-grids. An example is China, which is currently one of the greatest powers in HVDC transmission, and is also developing the first HVDC grid in the world:

Zhangbei grid [3]. In Europe, the option of the Pan-European Super-Grid has also been discussed [2], which would allow the massive integration of renewable energies in a system that would interconnect all Europe and North Africa.

1.2 Motivation

The objective of this thesis is to demonstrate the definition of the optimal HVDC system for a specific test system, based on the study of the optimal power flow (OPF) for different scenarios. Under these optimal operating conditions, with minimum losses, the results for different DC configurations are compared. In addition to showing that the OPF results are the ones with the lowest losses compared with different power flow (PF) simulations for the same test system.

The optimal power flow is an optimization problem applied in the field of electrical power systems. The calculation of the OPF for an electrical system allows solving its power flow, optimizing its operating conditions and adjusting the parameters of the control variables, without unfulfilling any of the system's constraints. Optimal operation of a power system allows to reduce costs, improve its efficiency and have more reliability.

In order to calculate the OPF, MatPower [4], an open-source Matlab based program is used for solving steady-state power system simulation and optimization problems. Matpower's problem is that it is only capable of calculating the OPF applied to AC systems, so it is necessary to develop an extension that allows the calculation of the OPF for hybrid AC/DC grids.

In this way, the modeling of a hybrid network is first developed, adding the HVDC system and the converter stations to the existing AC system. For the HVDC system, its power flow is studied from the definition of the losses in its transmission lines. For the converter stations, their conversion capacity, losses and master-slave control system are analyzed. From the modeling, an OPF mathematical model is developed, that allows simulating the operation of the system based on different constraints and through the definition of its state variables. And all this, with an objective function that minimizes the global losses of the system.

From the defined OPF model, and once the Matpower extension has been developed, the simulations for a test system are carried out. This makes possible to demonstrate the correct operation of the extension, apart from analyzing the impact of the HVDC sub-system on the system’s global operation.

2 HVDC and hybrid AC/DC grids

High Voltage Direct Current (HVDC) is an electrical energy transmission technology used to transport large powers over long distances. Under these conditions, HVDC lines offer lower energy losses, better reliability and a good economic balance, compared to HVAC lines. HVDC transmission is also widely used in underground or underwater lines, for which it is significantly more efficient than its AC competitor in both energy and economic aspects.

HVDC electric transmission technology currently has application in on-shore systems based on long-distance OHL and underground lines; and also in off-shore applications, for example, for underwater connections of off-shore wind farms or islands with a terrestrial network. HVDC transmission lines also allow the connection of two or more asynchronous or different frequency AC networks [5, 6].

2.1 History of HVDC

The first transmission line using DC was developed in 1882 between the German cities of Miesbach and Munich, and was only capable of transporting 1.5 kW across the 40 km. That same decade, the Swiss engineer René Thury developed a DC power transmission system based on an electromechanical principle from the connection of several motor-generator groups. By the end of the 1920s there were already fifteen Thury systems in operation; among which was the one developed in Italy by the Ferrari-Galliera company (the first of all of them, inaugurated in 1889, and capable of transporting up to 630 kW at 5 kV) and the Moutiers-Lyon System (with a maximum transmission of 8.6 MW from a hydroelectric plant) [7].

Starting in 1920, a new DC electrical transport technology based on mercury arc valves began to develop. The first transmission line based on this technology was designed for Berlin (Germany) but was never completed. After the World War II, the Soviet Union and Sweden resumed the studies. In 1951 the Moscow-Kashira System was inaugurated and in 1954 the Gotland System was put into operation, linking the mainland of Sweden and the island of Gotland; these being the first commercial systems based on mercury arc valves in operation. The Gotland System was capable of managing 20 MW at 100 kV through OHL and underwater lines [5, 8]. Until 1970s the most common DC transmission systems were those based on mercury arc valves. During these years, the most relevant project was the PDCI (Pacific HVDC Intertie), with a capacity that evolved from 1.5 GW to 3.1 GW through the years; and which remained in operation until 2004, when the valves were replaced by a new generation conversion system [8].

At the end of the 1970s, a new HVDC transmission technology began to be used where thyristors were incorporated in the converters; this technology will be known as LCC (Line-Commutated Converter), since they take the reference of an external AC system [5]. In 1979, a 1410 km HVDC-LCC transmission line began to operate between Johannesburg (South Africa) and Cahora Bassa (Mozambique) with a capacity of 1.92 GW at 533 kV [9]. Until the 2010s it was the most common technology; with projects like the Basslink line (Australia), that has been interconnecting the Australian continent with the island of Tasmania since 2006 [6, 10].

In 1997, the first experimental HVDC transmission line based on voltage-source converters (HVDC-VSC) was inaugurated, leaving behind the use of thyristors to start working with IGBTs in the converters, leading to a reduction in investment and maintenance costs of HVDC systems. Currently, VSC-based transmission systems occupy a big part of the HVDC market, especially among new implementation projects [6].

2.2 Comparison between HVDC and HVAC transmission

To define the points for and against the implementation of these HVDC transmission lines, the advantages and disadvantages of the HVDC lines with respect to the HVAC lines will be developed.

2.2.1 Advantages of HVDC transmission

The first of the advantages of using HVDC transmission lines is economic, since the investment costs have a critical distance from which the development of an HVDC line is profitable. Although the installations (transformer station, additional filters, etc.) of this type of transmission system represent an extra cost, the savings in cabling for HVDC transmission and the reduction in electrical losses allow the HVDC lines to be economically profitable for long distances. The critical distance from which the implementation of an overhead HVDC line is economically favorable is between 300 km and 400 km; while for an underwater line it is around 100 km [2, 6]. Figure 2.1 shows a graphic about the critical point for an underwater HVDC transmission line located between two converter stations.

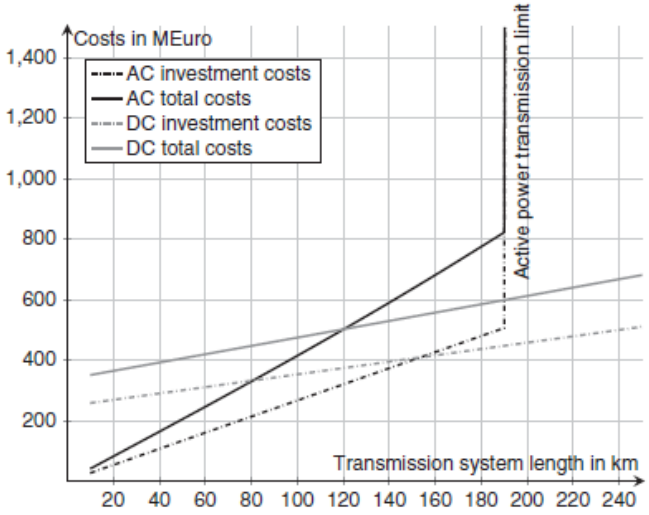

Figure 2.1: Cost comparison between AC and DC underwater transmission [2].

On the other hand, there are no losses in HVDC lines due to skin effect, and those related to corona effect are highly reduced. All this means that, in general, HVDC lines have significantly lower losses than HVAC lines for long distance transmissions systems, adding also the fact that the losses due to the Joule effect are reduced by the characteristics of the DC from Ohm's law [2, 11].

In addition, the absence of inductance allows HVDC lines to maintain good voltage regulation, offering better controllability than AC systems. HVDC lines also allow the interconnection of asynchronous or different frequency lines, since it decouples AC systems from each other. The null frequency of HVDC lines also entails less impact on nearby communication lines [6].

2.2.2 Disadvantages of HVDC transmission

The first disadvantage of HVDC lines compared to HVAC lines, is that maintenance costs may be higher (since more components are required in the system); and that an additional cost must also be considered for the continuous control of the line terminals, for which more expensive protections are required than in the case of AC.

In locations close to the conversion stations of the HVDC systems, the communication lines may be affected by radio noise generated by the high switching operation frequencies of the converters. Finally, for underground and underwater monopole HVDC systems, currents through the ground can cause electrocorrosion to pipelines and other underground metal installations [6].

2.3 HVDC technologies

This section introduces the two most common technologies of converter stations associated with the HVDC systems: conventional or LCC converter stations and VSC converter stations.

2.3.1 LCC converter stations

Conventional or LCC converter stations are characterized by having power converters based on thyristors. The main advantage of this technology is that it can manage very high power levels (up to between 6 and 7 GW) at voltages up to 800 kV [2, 6]. It should also be noted that it is a mature technology and that it has lower conversion losses than VSC technology. Figure 2.2 shows a comparison of the losses of a 1000-MW OHL connection for the different conversion technologies depending on the length of the line.

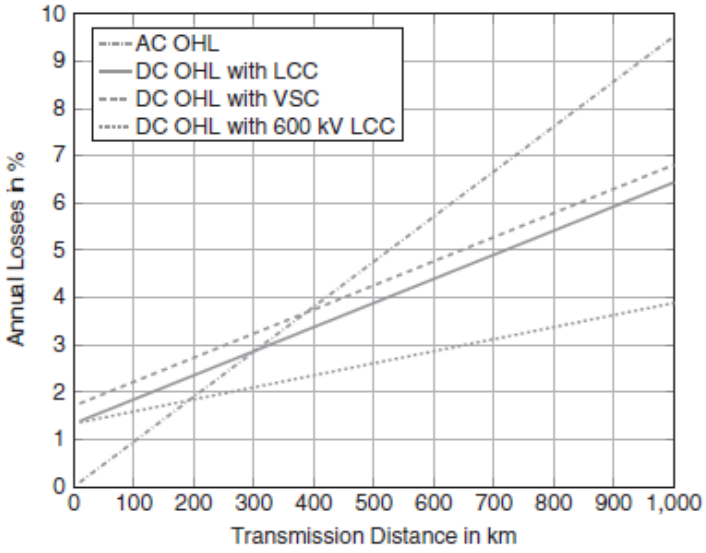

Figure 2.2: Line losses comparison between HVDC different technologies and HVAC [2].

The negative fact in the use of thyristors is that they only allow the control of the turning on, so only the active power can be controlled; while for the control of the reactive power it is necessary to have big capacitor banks that deliver the reactive power demanded by the station (between 50% and 60% of the nominal power). This means that the converter stations are large, which entails a space cost to be taken into account in applications, for example, like off-shore wind farms [6].

2.3.2 VSC converter stations

Converter stations with VSC technology have two-level, three-level or multilevel converters based on IGBT transistors. Figure 2.3 shows the scheme of an HVDC-VSC transmission system that connects two AC networks.

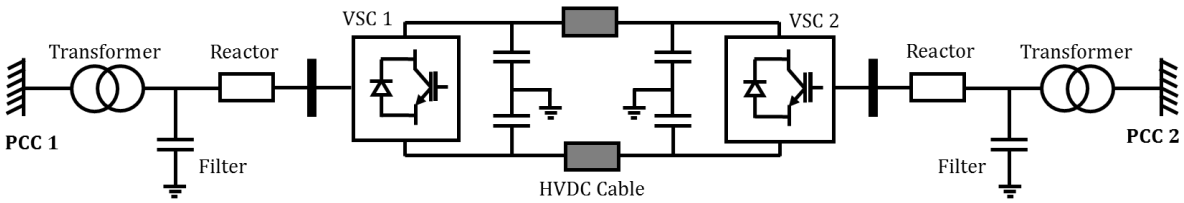

Figure 2.3: HVDC-VSC transmission system that connects two AC networks.

The maximum power managed by HVDC-VSC converter stations is currently 1.2 GW, with an operating voltage up to 320 kV. This means that for an HVDC transmission line there are sets of converter stations that supply the line which, due to the technical characteristics of the cabling, can transport up to 7.2 GW at 800 kV in OHL or 2.5 GW at 500 kV in underground systems [2]. With all this, different studies are currently in the development phase with the objective of having higher HVDC-VSC conversion power systems.

An advantage of this technology is that it offers a fast response and a low level of harmonics, which leads to the need of smaller filters than in the case of LCCs, thus reducing the necessary dimensions of the station. Another advantage is that HVDC-VSC has independent active and reactive power control, considerably reducing the reactive power to be delivered from capacitor banks [5, 6].

On the other hand, VSC technology presents significant losses associated with the high switching frequencies of the converters, which can also cause electromagnetic interference in the converter stations nearby [6].

3 Hybrid AC/DC grid modelling

In this chapter of the project, the mathematical model that defines a hybrid AC/DC grid is presented, including the AC power system, the DC power system and the converter stations that interconnect them. For the AC system, the modelling of its transmission lines (or branches) is presented and the nodal power balance is analyzed. For the DC system, the modelling of its HVDC transmission lines and the DC power flow is developed. The structure, losses, conversion capacity and control system of the converter stations are defined.

3.1 AC power system modelling

The AC power system is based on a set of nodes (or buses) where generators and loads can be connected. The nodes can be in communication with each other through transmission lines. For each of these nodes i, the complex voltage in magnitude and angle ($\overrightarrow{U_i} = U_i \angle \theta_i$) and the injected power ($\overrightarrow{S_i} = P_i + jQ_i$) must be known or obtained; P_i and Q_i being the active and reactive power injected into bus i.

3.1.1 AC branches modelling

The AC transmission lines are modelled from a π-equivalent structure [2]. The transmission line connecting AC buses i and j can be modelled from an impedance $Z_{\mathrm{L},ij} = R_{\mathrm{L},ij} + jX_{\mathrm{L},ij}$ (where $R_{\mathrm{L},ij}$ and $X_{\mathrm{L},ij}$ are the resistive and inductive components of the impedance), and a shunt admittance $Y_{\mathrm{q},ij} = G_{\mathrm{q},ij} + jB_{\mathrm{q},ij}$ (divided into a shunt conductance $G_{\mathrm{q},ij}$ and a shunt susceptance $B_{\mathrm{q},ij}$); as presented in Figure 3.1.

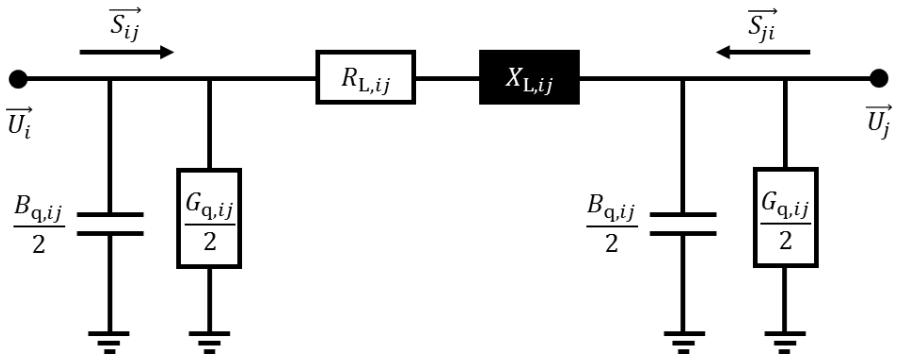

Figure 3.1: π-equivalent model for the transmission line.

When the power flow of the transmission line flows from node j to node i, and therefore power is injected to bus i, the power $\overrightarrow{S_{ij}}$ will take a negative value, while the power $\overrightarrow{S_{ji}}$ will be positive.

In order to build the network admittance matrix ($\mathrm{Y_{busAC}}$), each of the components of that matrix is calculated from the definition of the equivalent admittance of each branch ($y_{\mathrm{busAC},ij}$). To calculate these equivalent admittances, it is necessary to base on the equivalent model of AC transmission line discussed, as shown in Equation 1 [12, 13].

$$\mathrm{Y_{busAC}} = \begin{cases} y_{\mathrm{busAC},ii} = \sum_{n} \left(\frac{1}{Z_{\mathrm{L},ij}} + Y_{\mathrm{q},ij} \right) \\ y_{\mathrm{busAC},ij} = -\sum_{n} \frac{1}{Z_{\mathrm{L},ij}} \quad ; \quad \text{when } i \neq j \end{cases} \tag{1}$$

With this, it is possible to calculate the active and reactive power injected to node i by the transmission lines with which it is connected to the different buses j. For this, we will use Equations 2 and 3 [2, 14]; where U_i and U_j are the magnitudes and θ_i and θ_j the angles of the voltages on buses i and j, respectively. It should be noted that $G_{\mathrm{busAC},ij}$ and $B_{\mathrm{busAC},ij}$ refer to the conductance and susceptance that make up the equivalent admittance of the line ($y_{\mathrm{busAC},ij} = G_{\mathrm{busAC},ij} + jB_{\mathrm{busAC},ij}$) located between bus i and bus j.

$$P_{\sum \mathrm{br},i} = \sum_{j=1}^{n_{ac}} U_i \cdot U_j \cdot \left[G_{\mathrm{busAC},ij} \cdot \cos(\theta_i - \theta_j) + B_{\mathrm{busAC},ij} \cdot \sin(\theta_i - \theta_j) \right] \tag{2}$$

$$Q_{\sum \mathrm{br},i} = \sum_{j=1}^{n_{ac}} U_i \cdot U_j \cdot \left[G_{\mathrm{busAC},ij} \cdot \sin(\theta_i - \theta_j) - B_{\mathrm{busAC},ij} \cdot \cos(\theta_i - \theta_j) \right] \tag{3}$$

3.1.2 AC nodal power balance

Once the power injected by the transmission lines has been defined, the power balance equations can be written for each of the buses. To do this, the power injected by the generators ($P_{\mathrm{G},i}$, $Q_{\mathrm{G},i}$), by the loads ($P_{\mathrm{L},i}$, $Q_{\mathrm{L},i}$) and by the transmission lines ($P_{\sum \mathrm{br},i}$, $Q_{\sum \mathrm{br},i}$) are defined for each node i. Furthermore, in order to manage an AC/DC hybrid power electrical system, the power injected by the converters on the AC bus i ($P_{\mathrm{s},i}$, $Q_{\mathrm{s},i}$) will also be considered [14].

For a node i, the active and the reactive power balance is defined as shown in Equations 4 and 5, respectively.

$$P_{\mathrm{G},i} - P_{\mathrm{L},i} - P_{\mathrm{s},i} - P_{\sum \mathrm{br},i} = 0 \tag{4}$$

$$Q_{\mathrm{G},i} - Q_{\mathrm{L},i} - Q_{\mathrm{s},i} - Q_{\sum \mathrm{br},i} = 0 \quad (5)$$

Each of the AC nodes will be part of one of the three existing bus types: PQ, PV or Slack. The classification of the nodes among these three types is necessary to define the equipment to which they are connected and the control parameters. The three types of bus commented are developed below [12, 15]:

- **PV Nodes.** They are those nodes whose voltage magnitude and injected active power are set by a controller. In this way, the voltage angle and the reactive power injected are taken as unknown and must be determined from the power flow calculation. What can be considered as valid equipment for a PV node are synchronous generators (as long as synchronous generators work within the operating limits) and renewable energy sources (only if the grid operator allows renewable generators to operate within a PQ-diagram given and the voltage can be controlled). The converter stations that interconnect an HVDC system with the AC network will also be taken as PV nodes.
- **PQ Nodes.** The nodes whose injected active and reactive power are known, and the value of the magnitude and angle of the complex voltage are unknown, are PQ nodes. The following equipment are considered as PQ buses: loads (since they are typically defined from a demand for active and reactive power, without taking into account the dependence on voltage) and renewable generators (only if the grid operator demands a fixed power factor or if renewable generators are asked to supply a certain reactive power).
- **Slack Nodes.** Slack buses are necessary to balance the active and reactive power mismatch, since for the rest of the system nodes (the PQ and the PV nodes) the injected active power is already defined in the network model. Therefore, for the Slack-nodes, the magnitude and angle of the complex voltage are set by a controller, while the value of injected active and reactive power is unknown. The largest generator (or the largest set of distributed generators) is usually taken as Slack, since it is the one that will see its voltage least affected by a balancing of power mismatch.

3.2 DC power system modelling

The power flow calculation for DC networks is developed in a similar way to that used for the case of conventional AC networks [16]. One of the differences is the fact that the losses in the

DC transmission lines are only associated with resistive losses, so the equivalent model is based on a resistance ($R_{\mathrm{dc},ij}$) located between the DC nodes i and j. Figure 3.2 shows the equivalent scheme of a DC transmission line, where $U_{\mathrm{dc},i}$ and $U_{\mathrm{dc},j}$ are the voltages of nodes i and j, respectively.

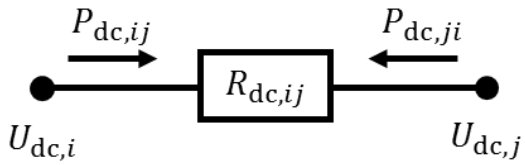

Figure 3.2: Equivalent model of the DC transmission line.

The power flow that flows from bus i to bus j ($P_{\mathrm{dc},ij}$) is negative when power is injected into bus i, while the power flow $P_{\mathrm{dc},ji}$ (from bus j to bus i) is positive in the same case, as can be seen in the previous figure.

The equivalent admittance of a DC transmission line connecting buses i and j is represented as $y_{\mathrm{dc},ij}$. When there is no transmission line between nodes i and j, a null admittance value is taken; and if nodes i and j are equivalent, an admittance equal to zero is also used. Equation 6 shows the calculation criterion for admittance $y_{\mathrm{dc},ij}$.

$$y_{\mathrm{dc},ij} = \begin{cases} 0\,, & \text{if no branch between nodes } i \text{ and } j \\ 0\,, & \text{if } i = j \\ \dfrac{1}{R_{\mathrm{dc},ij}} \end{cases} \tag{6}$$

From here, the admittance matrix of the DC network ($\mathrm{Y}_{\mathrm{busDC}}$) can be constructed from the definition of the different components that make it up ($y_{\mathrm{busDC},ij}$), as developed in Equation 7. There are two ways of determining the matrix component, depending on whether or not they are located on the diagonal of the admittance matrix.

$$\mathrm{Y}_{\mathrm{busDC}} = \begin{cases} y_{\mathrm{busDC},ii} = \sum_{j=1}^{\mathrm{N_{dc}}} y_{\mathrm{dc},ij} \\ y_{\mathrm{busDC},ij} = -y_{\mathrm{dc},ij} \;\; ; \;\; \text{when } i \neq j \end{cases} \tag{7}$$

From the matrix product between the admittance matrix and the voltage matrix in the DC bus j, the DC current injected to the DC line from node i can be calculated, as shown in Equation 8.

$$[I_{\mathrm{dc},i}] = [\mathrm{Y_{busDC}}] \cdot [U_{\mathrm{dc},j}] \tag{8}$$

With the current $I_{\mathrm{dc},i}$ determined, the calculation of the power that is injected into the transmission line from node i is carried out as shown in Equation 9.

$$P_{\mathrm{dc},i} = U_{\mathrm{dc},i} \cdot I_{\mathrm{dc},i} \tag{9}$$

Or in an equivalent way, developing the matrix calculation of the current flowing from node i, Equation 10 shows the calculation of the power injected into the line from bus i as a function of only $\mathrm{Y_{busDC}}$ and the voltages on buses i and j ($U_{\mathrm{dc},i}$ and $U_{\mathrm{dc},j}$) [2].

$$P_{\mathrm{dc},i} = U_{\mathrm{dc},i}^2 \cdot y_{\mathrm{busDC},ii} + U_{\mathrm{dc},i} \cdot \sum_{j \neq i} y_{\mathrm{busDC},ij} \cdot U_{\mathrm{dc},j} \tag{10}$$

3.3 Converter modelling

Figure 3.3 represents the general structure of a VSC-HVDC converter station [2]. It can be seen from the DC network that this converter station is made up of an inverter/rectifier converter, a phase reactor (represented as an impedance $\overrightarrow{Z_{\mathrm{c}}}$), an AC low-pass filter and a converter transformer.

The natural power flow of the converter is for the injection of power in the AC bus, which means that there is an input power from the DC side of the converter station defined by the voltage ($U_{\mathrm{dc},i}$) and the current ($I_{\mathrm{dc},i}$) at this point. At the AC bus i there is an active and a reactive power injected by the converter station ($P_{\mathrm{s},i}$ and $Q_{\mathrm{s},i}$, respectively) and a complex voltage with magnitude and angle ($\overrightarrow{U_{\mathrm{s},i}} = U_{\mathrm{s},i} \angle \theta_{\mathrm{s},i}$).

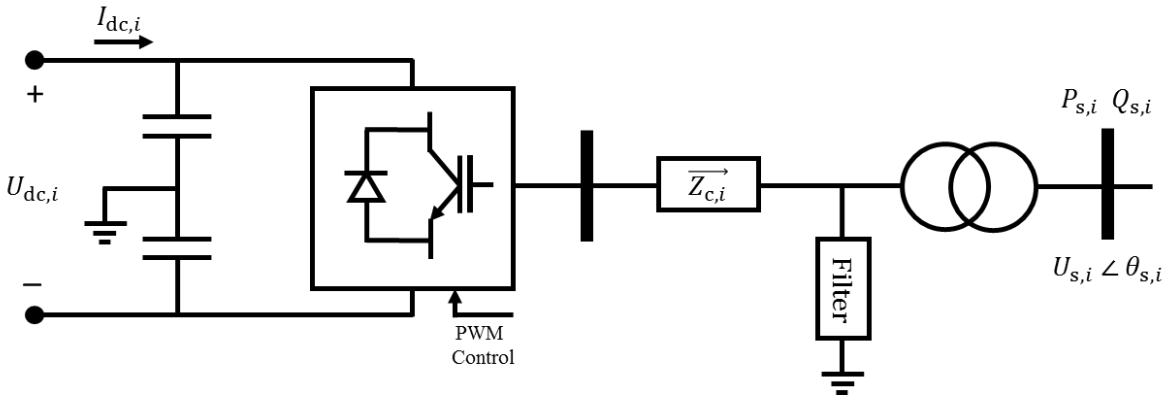

Figure 3.3: General structure of the converter station.

3.3.1 Converter station modelling

The converter station can be modelled as two controlled voltage sources, representing the inverter/rectifier converter: a complex voltage source for the AC side of the converter ($\overrightarrow{U_c} = U_c \angle \theta_c$, with magnitude and angle) and a direct voltage source for the DC side (U_{dc}). The phase reactor is represented as a complex impedance ($\overrightarrow{Z_c} = R_c + jX_c$, where R_c and X_c represent the resistive and inductive components of the phase reactor), the AC low pass filter is modelled as a susceptance (B_f) and the transformer converter is represented as another complex impedance ($\overrightarrow{Z_t} = R_t + jX_t$, where R_t and X_t represent the resistive and inductive components of the transformer).

Figure 3.4 shows the equivalent model of converter station connected to the AC bus i for a single-phase system based on the considerations discussed [2, 17].

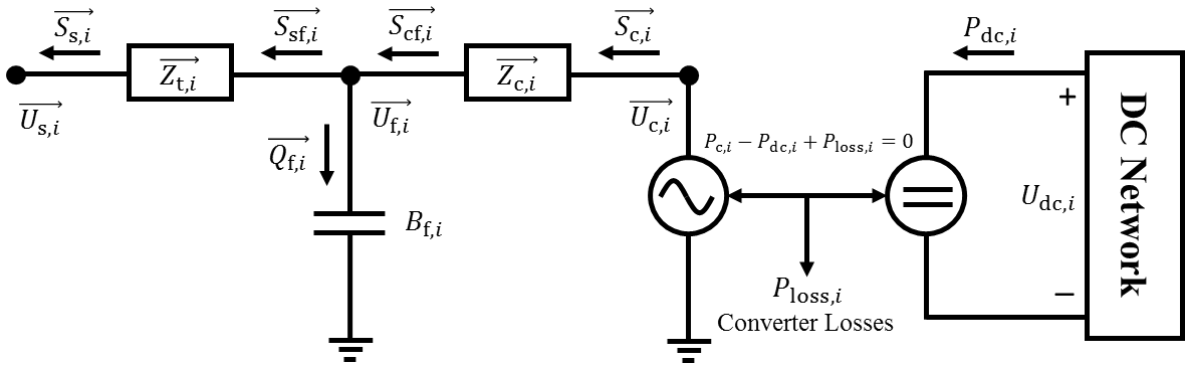

Figure 3.4: Equivalent model of the converter station for a single phase system.

3.3.2 Losses in the converter

The losses in the inverter/rectifier converter (P_{loss}) explain the difference between the input DC power to the converter (P_{dc}) and the AC output power of the converter (P_c). This loss factor refers to losses due to switching or conduction, among others. In this way, the power balance in the inverter/rectifier converter can be represented by Equation 11 [2, 14].

$$P_{c,i} - P_{dc,i} + P_{loss,i} = 0 \tag{11}$$

These losses in the converter can be calculated as presented in Equation 12, taking a quadratic dependence on the current flowing through the AC side of the converter (I_c);

$$P_{\text{loss},i} = a_i + b_i \cdot I_{\text{c},i} + c_i \cdot I_{\text{c},i}^2 \tag{12}$$

where, for each converters, the current on the AC side of the converter (I_c) can be calculated, as shown in Equation 13; from the quadratic summation of the active and reactive power on the AC side of the converter (P_c and Q_c), and the voltage at this same point (U_c).

$$I_{\text{c},i} = \frac{\sqrt{P_{\text{c},i}^2 + Q_{\text{c},i}^2}}{U_{\text{c},i}} \tag{13}$$

The individual loss factors a_i, b_i and c_i that define the losses in the converter refer to [16]:

- **No-load loss factor (a_i).** Transformers no-load losses and auxiliary equipment losses (such as lighting, refrigeration, control system, etc.).
- **Linear current factor (b_i).** Switching losses of the IGBTs and free-wheeling diodes.
- **Square current factor (c_i).** Conduction losses of the valves.

3.3.3 AC side of the converter modelling

Taking the AC side of the converter, shown in Figure 3.5, the objective of this section is to develop an equation system that relates the power on the AC side of the converter ($\overrightarrow{S_{\text{c},i}}$) and the power injected into the respective AC bus ($\overrightarrow{S_{\text{s},i}}$) [2, 14]; where $P_{\text{c},i}$ and $Q_{\text{c},i}$ are the active and reactive power on the AC side of the converter, and $P_{\text{s},i}$ and $Q_{\text{s},i}$ are the active and reactive power injected into the AC bus i from the converter station, respectively.

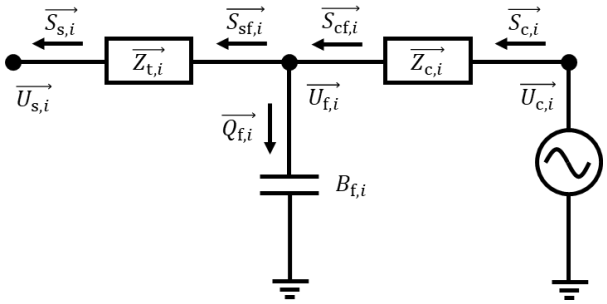

Figure 3.5: Equivalent model of the AC side of the converter for a single-phase system.

The set of equations that allows defining the different power flows that appear between the AC side of the converter and the AC bus are presented below. The power variables that appear in

this model are the power on the AC side of the converter ($\overrightarrow{S_{c,i}}$), the power at the output of the phase reactor ($\overrightarrow{S_{cf,i}}$), the reactive power absorbed by the filter ($Q_{f,i}$), the power at the transformer input ($\overrightarrow{S_{sf,i}}$), and the power injected into the AC bus ($\overrightarrow{S_{s,i}}$). All of them are made up of active and reactive parts, except for the power in the filter, which is a consumption only of reactive power.

All these defined powers have a direct dependence on the voltages that appear in the model. These are, defined with magnitude and angle, the voltage on the AC side of the converter ($\overrightarrow{U_c} = U_c \angle \theta_c$), the voltage across the filter ($\overrightarrow{U_f} = U_f \angle \theta_f$) and the AC bus voltage ($\overrightarrow{U_s} = U_s \angle \theta_s$).

The calculation of the active and reactive power injected into the AC bus by the converter station is based on Equations 14 and 15. It should be noted that $1/\overrightarrow{Z_{t,i}} = G_{t,i} + jB_{t,i}$, where $G_{t,i}$ is the conductance of the transformer and $B_{t,i}$ is its susceptance.

$$P_{s,i} = -U_{s,i}^2 \cdot G_{t,i} + U_{s,i} \cdot U_{f,i} \cdot \left[G_{t,i} \cdot \cos\left(\theta_{s,i} - \theta_{f,i}\right) + B_{t,i} \cdot \sin\left(\theta_{s,i} - \theta_{f,i}\right)\right] \quad (14)$$

$$Q_{s,i} = U_{s,i}^2 \cdot B_{t,i} + U_{s,i} \cdot U_{f,i} \cdot \left[G_{t,i} \cdot \sin\left(\theta_{s,i} - \theta_{f,i}\right) - B_{t,i} \cdot \cos\left(\theta_{s,i} - \theta_{f,i}\right)\right] \quad (15)$$

The active and reactive power on the AC side of the converter are calculated as shown below in Equations 16 and 17. It should be noted that $1/\overrightarrow{Z_{c,i}} = G_{c,i} + jB_{c,i}$, where $G_{c,i}$ is the conductance of the phase reactor and $B_{c,i}$ is its susceptance.

$$P_{c,i} = U_{c,i}^2 \cdot G_{c,i} - U_{f,i} \cdot U_{c,i} \cdot \left[G_{c,i} \cdot \cos\left(\theta_{f,i} - \theta_{c,i}\right) - B_{c,i} \cdot \sin\left(\theta_{f,i} - \theta_{c,i}\right)\right] \quad (16)$$

$$Q_{c,i} = -U_{c,i}^2 \cdot B_{c,i} + U_{f,i} \cdot U_{c,i} \cdot \left[G_{c,i} \cdot \sin\left(\theta_{f,i} - \theta_{c,i}\right) + B_{c,i} \cdot \cos\left(\theta_{f,i} - \theta_{c,i}\right)\right] \quad (17)$$

Equation 18 shows the calculation of the power in the filter. Considering null resistive losses, the power in the filter is reduced only to a reactive component.

$$Q_{f,i} = -U_{f,i}^2 \cdot B_{f,i} \quad (18)$$

Equations 19 and 20 are used to calculate the active and reactive power at the input of the transformer.

$$P_{sf,i} = U_{f,i}^2 \cdot G_{t,i} - U_{f,i} \cdot U_{s,i} \cdot \left[G_{t,i} \cdot \cos\left(\theta_{s,i} - \theta_{f,i}\right) - B_{t,i} \cdot \sin\left(\theta_{s,i} - \theta_{f,i}\right)\right] \quad (19)$$

$$Q_{sf,i} = -U_{f,i}^2 \cdot B_{t,i} + U_{f,i} \cdot U_{s,i} \cdot \left[G_{t,i} \cdot \sin\left(\theta_{s,i} - \theta_{f,i}\right) + B_{t,i} \cdot \cos\left(\theta_{s,i} - \theta_{f,i}\right)\right] \quad (20)$$

And finally, in order to obtain the power at the output of the phase reactor, the calculation is developed according to Equations 21 and 22.

$$P_{\mathrm{cf},i} = -U_{\mathrm{f},i}^2 \cdot G_{\mathrm{c},i} + U_{\mathrm{f},i} \cdot U_{\mathrm{c},i} \cdot \left[G_{\mathrm{c},i} \cdot \cos\left(\theta_{\mathrm{f},i} - \theta_{\mathrm{c},i}\right) + B_{\mathrm{c},i} \cdot \sin\left(\theta_{\mathrm{f},i} - \theta_{\mathrm{c},i}\right)\right] \quad (21)$$

$$Q_{\mathrm{cf},i} = U_{\mathrm{f},i}^2 \cdot B_{\mathrm{c},i} + U_{\mathrm{f},i} \cdot U_{\mathrm{c},i} \cdot \left[G_{\mathrm{c},i} \cdot \sin\left(\theta_{\mathrm{f},i} - \theta_{\mathrm{c},i}\right) - B_{\mathrm{c},i} \cdot \cos\left(\theta_{\mathrm{f},i} - \theta_{\mathrm{c},i}\right)\right] \quad (22)$$

In the case of VSC-MMC converter stations, with or without a small AC filter, the model presented according to Figure 3.5 can be simplified [2, 18]. In this way, the equivalent model of the AC side of the inverter without a filter can be represented as shown in Figure 3.6; with $\overrightarrow{Z_{\mathrm{tc},i}} = \overrightarrow{Z_{\mathrm{t},i}} + \overrightarrow{Z_{\mathrm{c},i}}$, where $\overrightarrow{Z_{\mathrm{tc},i}}$ is the equivalent impedance for the AC side of the converter without filter.

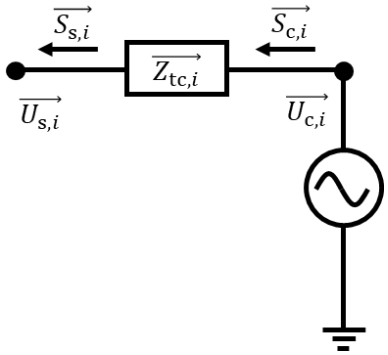

Figure 3.6: Equivalent model of the AC side of the converter for a single-phase system without filter.

With this, the calculations of the power on the AC side of the converter ($\overrightarrow{S_{\mathrm{c},i}}$) and the power injected into the AC bus ($\overrightarrow{S_{\mathrm{s},i}}$) will only depend on the complex voltages in these same points ($\overrightarrow{U_{\mathrm{c}}}$ and $\overrightarrow{U_{\mathrm{s}}}$, respectively). Equations 23 and 24 show the calculation of the active and reactive power injected into the AC bus i. It is considered that $1/\overrightarrow{Z_{\mathrm{tc},i}} = G_{\mathrm{tc},i} + jB_{\mathrm{tc},i}$, where $G_{\mathrm{tc},i}$ is the conductance of the transformer and the phase reactor set and $B_{\mathrm{tc},i}$ is its susceptance.

$$P_{\mathrm{s},i} = -U_{\mathrm{s},i}^2 \cdot G_{\mathrm{tc},i} + U_{\mathrm{s},i} \cdot U_{\mathrm{c},i} \cdot \left[G_{\mathrm{tc},i} \cdot \cos\left(\theta_{\mathrm{s},i} - \theta_{\mathrm{c},i}\right) + B_{\mathrm{tc},i} \cdot \sin\left(\theta_{\mathrm{s},i} - \theta_{\mathrm{c},i}\right)\right] \quad (23)$$

$$Q_{\mathrm{s},i} = U_{\mathrm{s},i}^2 \cdot B_{\mathrm{tc},i} + U_{\mathrm{s},i} \cdot U_{\mathrm{c},i} \cdot \left[G_{\mathrm{tc},i} \cdot \sin\left(\theta_{\mathrm{s},i} - \theta_{\mathrm{c},i}\right) - B_{\mathrm{tc},i} \cdot \cos\left(\theta_{\mathrm{s},i} - \theta_{\mathrm{c},i}\right)\right] \quad (24)$$

On the other hand, Equations 25 and 26 develop the calculation of the active and reactive power on the AC side of the converter.

$$P_{\mathrm{c},i} = U_{\mathrm{c},i}^2 \cdot G_{\mathrm{tc},i} - U_{\mathrm{s},i} \cdot U_{\mathrm{c},i} \cdot \left[G_{\mathrm{tc},i} \cdot \cos\left(\theta_{\mathrm{s},i} - \theta_{\mathrm{c},i}\right) - B_{\mathrm{tc},i} \cdot \sin\left(\theta_{\mathrm{s},i} - \theta_{\mathrm{c},i}\right)\right] \quad (25)$$

$$Q_{c,i} = -U_{c,i}^2 \cdot B_{tc,i} + U_{s,i} \cdot U_{c,i} \cdot \left[G_{tc,i} \cdot \sin\left(\theta_{s,i} - \theta_{c,i}\right) + B_{tc,i} \cdot \cos\left(\theta_{s,i} - \theta_{c,i}\right)\right] \quad (26)$$

This simplification is used for the final model developed in this work, since the converters considered apply modular multilevel converter (MMC) technology. Whether they have small filters or no filter at all, this simplification can be considered good enough for reliable results.

3.3.4 Converter control system

The most common control system applied to VSC converter stations in MTDC systems (and also applicable to MMC converter stations) is based on the architecture shown in Figure 3.7. It consists of a set of inner control loops and outer control loops that allow the control of power and voltage from defined reference values. The controlled voltage source characteristics of the VSC converter allow control through a modulator. The architecture presented offers three control strategies: master-slave control, voltage margin control and DC-voltage droop control. This project will only focus on the master-slave strategy [18–20].

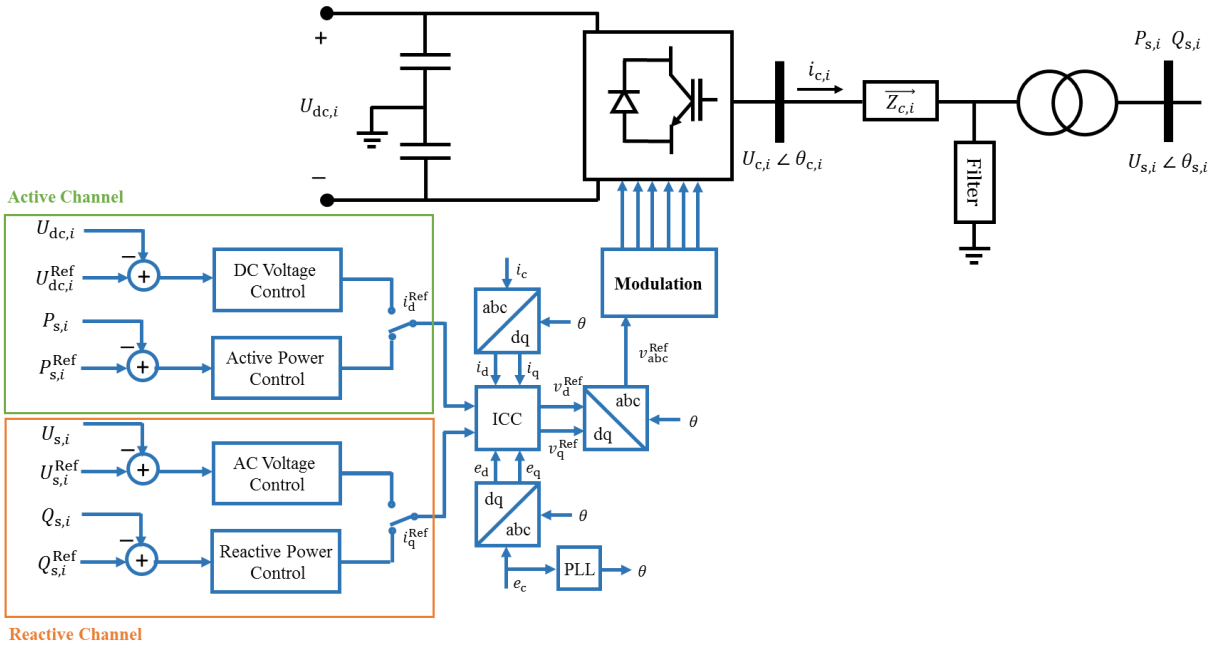

Figure 3.7: Common architecture of the control system for a VSC-HVDC station.

In a control system based on the architecture presented above, there are two channels: the active channel and the reactive channel. The active channel is responsible for regulating DC voltage or active power, while the reactive channel is responsible for controlling the amplitude

of the AC voltage or reactive power. For each converter station to be controlled in an AC/DC system, it must be decided which variable needs to be controlled for each channel. In the case of the master-slave control strategy, a single master converter station is assigned to control the DC voltage profile in an MTDC system, while the rest of the VSC stations, the slave stations, regulate the power.

In the case of the master converter station, the active current is controlled from the variation of the power. Through its active control channel, it performs a constant DC voltage control by varying the active power. In its reactive channel, on the other hand, a constant AC voltage control is carried out, normally applied in connection with passive loads or wind farms, injecting or consuming reactive power. Thus, the operation and reliability of the entire AC/DC system depends on the correct operation of the control system in the master VSC station. To avoid negative effects on the AC grid and to allow a quick adaptation of the HVDC system, the master station should be connected to a strong AC grid. With this, Equations 27 and 28 show the control equations applied to the master converter station with the defined reference values [18].

$$U_{\mathrm{dc},i} - U_{\mathrm{dc},i}^{\mathrm{Ref}} = 0 \tag{27}$$

$$U_{\mathrm{s},i} - U_{\mathrm{s},i}^{\mathrm{Ref}} = 0 \tag{28}$$

The slave converter stations base their control system on a constant power control. This control method allows to regulate the active and reactive power separately. Equations 29 and 30 show the control equations applied to the slave converter station, for the active and reactive channel, respectively, with the defined reference values [18].

$$P_{\mathrm{s},i} - P_{\mathrm{s},i}^{\mathrm{Ref}} = 0 \tag{29}$$

$$Q_{\mathrm{s},i} - Q_{\mathrm{s},i}^{\mathrm{Ref}} = 0 \tag{30}$$

For the control of active and reactive power by the slave converter stations, Equations 31 and 32 are used in the d-q reference frame from the variables used in the control loop [20]. According to the nomenclature in figure 3.7, v_{d} and i_{d} refer to control voltage and current on the d-axis, while v_{q} and i_{q} refer to control voltage and current on the q-axis.

$$P_{\mathrm{control}} = v_{\mathrm{d}} \cdot i_{\mathrm{d}} + v_{\mathrm{q}} \cdot i_{\mathrm{q}} \tag{31}$$

$$Q_{\mathrm{control}} = v_{\mathrm{q}} \cdot i_{\mathrm{d}} - v_{\mathrm{d}} \cdot i_{\mathrm{q}} \tag{32}$$

Since the d-q reference frame is aligned with the phasor of the AC voltage through a PLL loop, these equations can be simplified to those shown in Equations 33 and 34 [20].

$$P_{\text{control}} = v_{\text{d}} \cdot i_{\text{d}} \tag{33}$$

$$Q_{\text{control}} = -v_{\text{d}} \cdot i_{\text{q}} \tag{34}$$

With all this, it is demonstrated that the control of VSC converter stations can be modelled from the definition of a reference value for the DC voltage and the AC output voltage for the master station, and a reference value for the active and reactive power in slave stations; according to Equations 27 to 30.

4 Optimal power flow

The optimal power flow is a non-linear and non-convex optimization problem applied in the field of electrical power systems. In the same way as in the calculation of a conventional power flow, the objective is to obtain a generation equivalent to the consumption (also taking into account all system losses). In this way, what differentiates the OPF calculation from the PF is that the optimal power flow not only offers a technically feasible solution, but also optimal; minimizing generation costs, losses, or any parameter defined in the target function. With this, the optimal power flow is useful to technically and economically evaluate the operation of an electrical power system.

As mentioned, the OPF model has a target or objective function that allows obtaining optimal operating conditions for the electrical power system studied around the technical or economic parameters defined in this function. The objective function, dependent on all state variables x, is shown below in a generic format. It should be noted that the objective function can be presented as a linear, piece-wise linear or polynomial function [12, 14, 21].

$$\min_x f(x) \tag{35}$$

In addition to the target function, there must also be a set of equality and inequality constraints that allow mathematically defining the characteristics of the system, its technical limits and the impositions of the grid operator. The generic formulation for these constraints is shown below, respectively are equality constraints, inequality constraints (non-linear and linear) and bounds for the state variables.

$$g(x) = 0 \tag{36}$$

$$h(x) \leq 0 \tag{37}$$

$$l \leq A \cdot x \leq u \tag{38}$$

$$x_{Min} \leq x \leq x_{Max} \tag{39}$$

The vectors that contain all the non-linear equality and inequality constraints are those presented in Equations 36 and 37, respectively. Equation 38 shows the format in which the linear equality and inequality constraints are defined, where A is a matrix with constant values that multiplies the set of variables, and u and l are the upper and lower limits, which in the case of the linear equality constraints both take the same value. Equation 39 presents the bounds for the state variables, imposing a maximum and a minimum value for each of them.

4.1 Lagrangian method

From the defined optimization problem, with a total of n_{eq} equality constraints $g(x)$ and n_{ineq} inequality constraints $h(x)$, the Lagrangian method can be applied to obtain the optimal result. The idea of the Lagrangian method is to take into account the constraints by adding them to the objective function $f(x)$, weighted by the Lagrangian multipliers (λ and μ), as shown in Equation 40 [12, 21]. The application of the Lagrangian method allows the subsequent use of optimization methods such as Newton-Raphson, since the dual function dependent on x, λ and μ (Equation 40) will always be concave, even when $f(x)$, $g(x)$ or $h(x)$ are not.

$$L(x,\lambda,\mu) = f(x) + \sum_{i=1}^{n_{\text{eq}}} \lambda_i \cdot g_i(x) + \sum_{j=1}^{n_{\text{ineq}}} \mu_i \cdot h_i(x) \tag{40}$$

With all this, the objective of the Lagrangian multipliers is to define the Lagrangian function as a concave function, and taking the smallest feasible value that allows obtaining the optimal result. The dual variable λ refers to the relationship between the gradient of the objective function and the gradient of the equality constraints, while the dual variable μ relates the gradient of the objective function to the gradient of the inequality constraints. The Lagrangian multipliers can also be interpreted as linear barriers, since when a constraint is not fulfilled, they take an infinite value, and therefore they rule out that solution.

4.2 Solver

The solver used in this work is the MatPower Interior Point Solver (MIPS), which is a primal-dual interior point solver based on the optimization model presented at the beginning of this chapter [4]. Figure 4.1 shows the flowchart diagram that outlines the calculation process of the optimization problem developed by the solver [21].

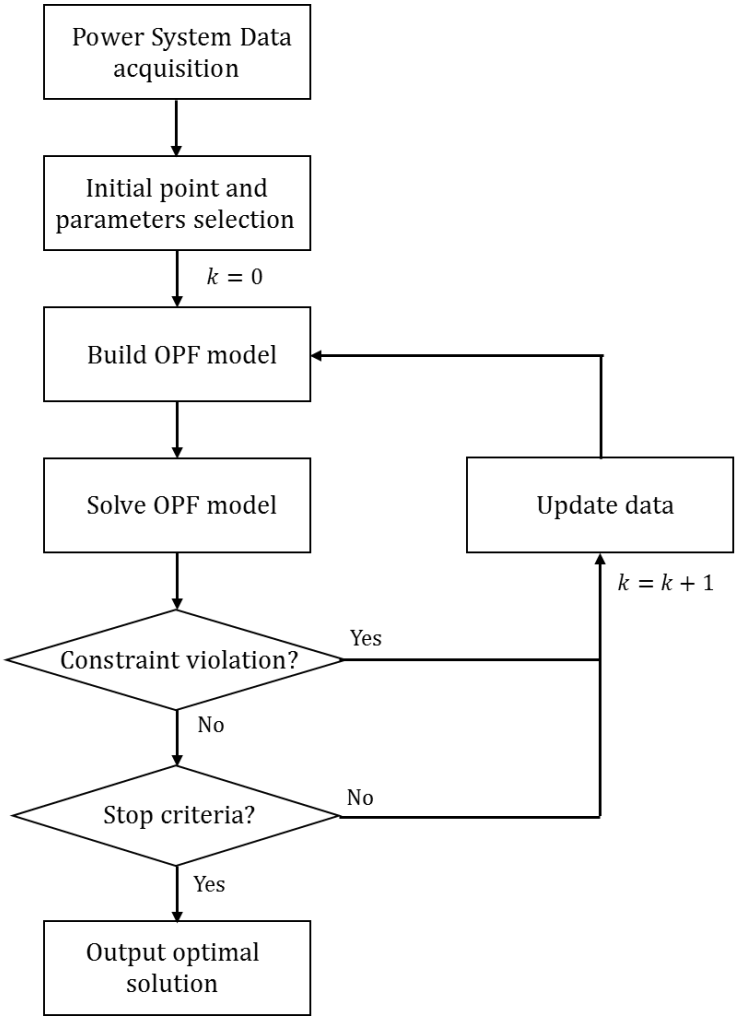

Figure 4.1: Flowchart diagram of the calculation process with MIPS.

The first step in the calculation process is the acquisition of the matrices that group the input data, from which the initial values for all the variables and the rest of the system parameters are defined for the initial iteration ($k = 0$). From here, the OPF model based on the hybrid grid modelling is defined and the problem is solved. If any of the constraints is violated, the OPF model is redefined with updated values for the variables (this being the $k = k + 1$ iteration); on the other hand, if none of the constraints has been unfulfilled, the next step is achieved. Next, if the stop criteria have been met, having reached the maximum number of iterations or having obtained the optimal result, the optimal solution is offered as output data matrices; if the stop criteria has not been met, a new iteration $k = k + 1$ is performed, updating the values of the variables.

5 Optimal power flow for AC/DC grids

In this section, the extension in the formulation related to the optimal power flow (OPF) for hybrid AC/DC networks is developed, based on the formulation used in MatPower for the calculation of OPF for AC electrical networks. To do this, the objective function is first redefined, for which the new variables and constraints are developed, including the DC system as addition to the existing one. The new variables and constraints are related to the DC transmission network, and the converters that interconnect DC and AC systems.

5.1 Objective function

The objective function is defined, in order to offer the value of each of the variables considered, so that the losses in the entire hybrid AC/DC network are minimal [14]. The losses in the system are directly related to the total power injected in all the nodes of the system. With this, the objective function to take into account in the defined OPF is presented in Equation 41.

$$[Min] \quad f\left(x^{\mathrm{T}}\right) = \sum_{i=1}^{\mathrm{N_{ac}}} P_i \tag{41}$$

In this objective function, P_i refers to the power injected into the AC bus i, for which the power injection of the generators (as a positive value), the power injection of the loads and converters (the latter being negative) are taken into account. However, it will be sought to obtain a minimum value for the sum of this injected power for all the AC nodes of the system ($\mathrm{N_{ac}}$). The vector x^{T} refers to the set of optimization variables that are taken into account, and that will be developed later.

5.2 Optimization variables

The optimization variables contained in the vector x^{T} are all those variables that influence the variation of the final value of the objective function. The vector x^{T} is presented in Equation 42 [14].

$$x^{\mathrm{T}} = \left[U, \theta, P_{\mathrm{G}}, Q_{\mathrm{G}}, P_{\mathrm{s}}, Q_{\mathrm{s}}, P_{\mathrm{c}}, Q_{\mathrm{c}}, P_{\mathrm{dc}}, U_{\mathrm{c}}, \theta_{\mathrm{c}}, U_{\mathrm{dc}}, U_{\mathrm{dc}}^{\mathrm{Ref}}, P_{\mathrm{s}}^{\mathrm{Ref}}, Q_{\mathrm{s}}^{\mathrm{Ref}}, U_{\mathrm{s}}^{\mathrm{Ref}}\right] \tag{42}$$

The state variables contained in the vector x^{T} are:

- The magnitude of the voltage on the AC buses (U)
- The angle of the voltage on the AC buses (θ)
- The active generation power associated with the AC nodes ($\mathrm{P_G}$)
- The reactive generation power associated with the AC nodes (Q_{G})
- The active power injected to the AC nodes from the converters (P_{s})
- The reactive power injected to the AC nodes from the converters (Q_{s})
- The active power in the AC side of the converter (P_{c})
- The reactive power in the AC side of the converter (Q_{c})
- The DC power flowing from the converter to the DC line (P_{dc})
- The magnitude of the voltage on the AC side of the converter (U_{c})
- The angle of the voltage on the AC side of the converter (θ_{c})
- The voltage on the DC buses (U_{dc})

In addition, and considering a control method based on the master-slave strategy, the control variables of the converters are:

- The reference voltage in DC ($U_{\mathrm{dc}}^{\mathrm{Ref}}$)
- The reference voltage in AC ($U_{\mathrm{s}}^{\mathrm{Ref}}$)
- The reference reactive power for the converters ($P_{\mathrm{s}}^{\mathrm{Ref}}$)
- The reference reactive power for the converters (Q_{s}^{Ref})

5.3 Equality constraints

The equality constraints shown in this section, refer to the equality constraints that are added or modified with respect to the AC OPF model, in order to obtain the OPF model for hybrid networks.

First, the modified nodal power balance is shown, which takes into account the power injection by the converters into the AC system. Operation constraints are also presented, which define

the converters and the HVDC system through, for example, the power flow in the DC transmission lines and in the converter stations, or the losses in those converter stations. Control constraints are also within equality constraints, whose operation is defined depending on whether the converter works as a master or slave converter.

5.3.1 Nodal power balance

The nodal power balance for each of the AC buses, defined in the section 3.1.2 of this work in its Equations 4 and 5, is the first of the equality constraints to be presented. According to these equations, Equation 43 shows the nodal power balance constraint for each node i [4], where the mismatch power (S_i^{bus}), the power demanded by the load ($S_{\text{L},i}$), the generated power at the synchronous generators ($S_{\text{G},i}$) and the power delivered from the converters ($S_{\text{S},i}$) appear. In addition, two binary variables are presented ($C_{\text{G},i}$ and $C_{\text{S},i}$) that define the operability or existence in each bus i of generators or converters, respectively.

$$G^S(X) = S_i^{\text{bus}} + S_{\text{L},i} - C_{\text{G},i} \cdot S_{\text{G},i} + C_{\text{S},i} \cdot S_{\text{S}.i} = 0 \tag{43}$$

The equality constraint $G^S(X)$ depends directly on the magnitude and angle of the complex voltage (V and θ), on the active and reactive power generated by the synchronous generators (P_{G} and Q_{G}) and on the active and reactive power delivered to the converters (P_{s} and Q_{s}), in each of the AC nodes. It is necessary to comment that this function is a non-linear constraint, since there is a non-linear dependency with respect to the variables that define it. With this, there will be a number of equality constraints based on $G^S(X)$ equal to the number of AC nodes that exist in the studied system.

In order to solve the optimization problem, it will be necessary to define the Jacobian and Hessian matrices for each of the non-linear constraints, as is the case of the current constraint, since they are part of the calculation process for the Lagrangian function, which is used for the MIPS for an optimization case. The first partial derivatives of the function $G^S(X)$ are presented, determined for each of the variables on which it depends. These first partial derivatives are defined in Appendix 1.1 [22, 23].

To simplify the nomenclature, the first partial derivatives for each of the variables are presented in the form shown in Equation 44, where X refers to the variable for which the partial derivative is calculated.

$$G_X^S = \frac{\partial G^S}{\partial X} \tag{44}$$

From these first partial derivatives, the Jacobian matrix can be constructed, which takes the shape presented in Equation 45. The Jacobian matrix for this constraint will have dimensions m x n, where the number of rows m is equal to the number of AC nodes (since for each one of the nodes, each variable takes different values) and the number of columns n is equal to the number of variables on which the constraint depends, which in the case of nodal power balance is equal to six.

$$G_X^S = \begin{bmatrix} G_\theta^S & G_V^S & G_{P_\mathrm{G}}^S & G_{Q_\mathrm{G}}^S & G_{P_\mathrm{s}}^S & G_{Q_\mathrm{s}}^S \end{bmatrix} \tag{45}$$

From here, the Hessian matrix can be calculated. The simplified nomenclature referring to the second partial derivatives of the function $G^S(X)$ is stated in Equation 46, where X can take the value of any of the variables on which the constraint depends.

$$G_{XX}^S = \frac{\partial G_X^S}{\partial X} \tag{46}$$

From all the second partial derivatives, the Hessian matrix can be constructed, which is presented in Equation 47. As can be seen, the two variables that appear under-indexed in each of the elements refer to the two variables for which the second partial derivative is defined. The dual variable λ is also added, which refers to the Lagrangian multiplier for equality constraints.

$$G_{XX}^S = \begin{bmatrix} G_{\theta\theta}^S(\lambda) & G_{\theta V}^S(\lambda) & G_{\theta P_\mathrm{G}}^S(\lambda) & G_{\theta Q_\mathrm{G}}^S(\lambda) & G_{\theta P_\mathrm{s}}^S(\lambda) & G_{\theta Q_\mathrm{s}}^S(\lambda) \\ G_{V\theta}^S(\lambda) & G_{VV}^S(\lambda) & G_{VP_\mathrm{G}}^S(\lambda) & G_{VQ_\mathrm{G}}^S(\lambda) & G_{VP_\mathrm{s}}^S(\lambda) & G_{VQ_\mathrm{s}}^S(\lambda) \\ G_{P_\mathrm{G}\theta}^S(\lambda) & G_{P_\mathrm{G}V}^S(\lambda) & G_{P_\mathrm{G}P_\mathrm{G}}^S(\lambda) & G_{P_\mathrm{G}Q_\mathrm{G}}^S(\lambda) & G_{P_\mathrm{G}P_\mathrm{s}}^S(\lambda) & G_{P_\mathrm{G}Q_\mathrm{s}}^S(\lambda) \\ G_{Q_\mathrm{G}\theta}^S(\lambda) & G_{Q_\mathrm{G}V}^S(\lambda) & G_{Q_\mathrm{G}P_\mathrm{G}}^S(\lambda) & G_{Q_\mathrm{G}Q_\mathrm{G}}^S(\lambda) & G_{Q_\mathrm{G}P_\mathrm{s}}^S(\lambda) & G_{Q_\mathrm{G}Q_\mathrm{s}}^S(\lambda) \\ G_{P_\mathrm{s}\theta}^S(\lambda) & G_{P_\mathrm{s}V}^S(\lambda) & G_{P_\mathrm{s}P_\mathrm{G}}^S(\lambda) & G_{P_\mathrm{s}Q_\mathrm{G}}^S(\lambda) & G_{P_\mathrm{s}P_\mathrm{s}}^S(\lambda) & G_{P_\mathrm{s}Q_\mathrm{s}}^S(\lambda) \\ G_{Q_\mathrm{s}\theta}^S(\lambda) & G_{Q_\mathrm{s}V}^S(\lambda) & G_{Q_\mathrm{s}P_\mathrm{G}}^S(\lambda) & G_{Q_\mathrm{s}Q_\mathrm{G}}^S(\lambda) & G_{Q_\mathrm{s}P_\mathrm{s}}^S(\lambda) & G_{Q_\mathrm{s}Q_\mathrm{s}}^S(\lambda) \end{bmatrix} \tag{47}$$

Substituting all those null second derivatives in the matrix, it can be simplified as presented in Equation 48. In this way, the dimensions of the Hessian matrix of the nodal power balance will again depend on the number of AC nodes that the studied system has, plus all defined null elements. For example, in a system with 10 AC nodes, 3 generators and 2 converters, each of the non-zero elements ($G_{\theta\theta}^S(\lambda)$, $G_{V\theta}^S(\lambda)$, $G_{\theta V}^S(\lambda)$, $G_{VV}^S(\lambda)$) will take on 10x10 dimensions, so the

Hessian matrix will have 30x30 dimensions (since P_G and Q_G have 3 values each, and P_s and Q_s have 2), being always a square matrix [22, 23].

$$G_{XX}^{S} = \begin{bmatrix} G_{\theta\theta}^{S}(\lambda) & G_{\theta V}^{S}(\lambda) & 0 & 0 & 0 & 0 \\ G_{V\theta}^{S}(\lambda) & G_{VV}^{S}(\lambda) & 0 & 0 & 0 & 0 \\ 0 & 0 & 0 & 0 & 0 & 0 \\ 0 & 0 & 0 & 0 & 0 & 0 \\ 0 & 0 & 0 & 0 & 0 & 0 \\ 0 & 0 & 0 & 0 & 0 & 0 \end{bmatrix} \tag{48}$$

The second partial derivatives referred to the non-zero elements of the Hessian matrix are defined in Appendix 1.1.

5.3.2 Power flow in the DC system

This second constraint defines the DC power flow through the HVDC transmission lines. It is again a non-linear equality constraint, as can be verified in Equation 49, since it has a non-linear dependence with respect to the variables on which it depends: the DC voltage (U_{dc}) and the DC power flowing to the DC line from the converter (P_{dc}). This constraint is based on Equation 10 from section 3.2, which defines the power flow in the DC system, and which is calculated from the DC voltage and the admittance matrix (Y_{busDC}) between the DC nodes i and j.

$$G^{P_{dc}}(X) = U_{dc,i}^{2} \cdot y_{busDC,ii} + U_{dc,i} \cdot \sum_{j \neq i} y_{busDC,ij} \cdot U_{dc,j} - P_{dc,i} = 0 \tag{49}$$

As it is a non-linear equality constraint, it is necessary to have Jacobian and Hessian matrices to solve the optimization problem. To define the Jacobian matrix, it is necessary to determine the first partial derivatives. Equation 50 shows the simplification in the nomenclature to refer to the first partial derivatives. Into the state variable U_{dc}, two operation variables will be differentiated: the DC bus voltage on the origin bus ($U_{dc,i}$) and on the destination bus ($U_{dc,j}$) of the power flow.

$$G_{X}^{P_{dc}} = \frac{\partial G^{P_{dc}}}{\partial X} \tag{50}$$

The first partial derivatives of the constraint $G^{P_{dc}}(X)$ are presented below, in Equations 51 to 53. As can be seen, Equation 51 will allow us to define the values located on the diagonal of

the matrix of the first derivatives, while Equation 52 allows to calculate the value of the elements that are outside the diagonal of this matrix [16]. On the other hand, Equation 53 shows the first derivative as a function of P_{dc}.

$$G^{P_{\mathrm{dc}}}_{U_{\mathrm{dc},i}} = 2 \cdot y_{\mathrm{busDC},ii} \cdot U_{\mathrm{dc},i} + \sum_{j \neq i} y_{\mathrm{busDC},ij} \cdot U_{\mathrm{dc},j} \quad ; \quad \text{with } j = i \tag{51}$$

$$G^{P_{\mathrm{dc}}}_{U_{\mathrm{dc},j}} = y_{\mathrm{busDC},ij} \cdot U_{\mathrm{dc},i} \quad ; \quad \text{with } j \neq i \tag{52}$$

$$G^{P_{\mathrm{dc}}}_{P_{\mathrm{dc}}} = -1 \tag{53}$$

The Jacobian matrix defined for the non-linear equality constraint $G^{P_{\mathrm{dc}}}(X)$ is presented in Equation 54. As it only depends on two state variables (U_{dc} and P_{dc}), the Jacobian matrix will have two columns; while the number of rows will depend on the number of converters that the studied system has.

$$G^{P_{\mathrm{dc}}}_{X} = \begin{bmatrix} G^{P_{\mathrm{dc}}}_{U_{\mathrm{dc}}} & G^{P_{\mathrm{dc}}}_{P_{\mathrm{dc}}} \end{bmatrix} \tag{54}$$

The next step is to define the Hessian matrix, for which the different second partial derivatives have to be calculated. Equation 55 shows the simplified nomenclature for referring to these second partial derivatives.

$$G^{P_{\mathrm{dc}}}_{XX} = \frac{\partial G^{P_{\mathrm{dc}}}_{X}}{\partial X} \tag{55}$$

For the definition of second derivatives, two equations are now again distinguished: Equation 56 is used to calculate the elements located on the diagonal of the matrix, while Equation 57 refers to the calculation of the elements that are located off the diagonal of the matrix [16]. From here, the commented set of equations will allow to obtain the final matrix of second derivatives $G^{P_{\mathrm{dc}}}_{XX}$ only as a function of the state variable U_{dc}. All second derivatives where P_{dc} is involved are equal to zero.

$$G^{P_{\mathrm{dc}}}_{U_{\mathrm{dc},i}U_{\mathrm{dc},i}} = \frac{\partial P_{\mathrm{dc},i}}{\partial U^2_{\mathrm{dc},i}} = 2y_{\mathrm{dc},ii} \quad ; \quad \text{with } j = i \tag{56}$$

$$G^{P_{\mathrm{dc}}}_{U_{\mathrm{dc},i}U_{\mathrm{dc},j}} = \frac{\partial P_{\mathrm{dc},i}}{\partial U_{\mathrm{dc},i} \partial U_{\mathrm{dc},j}} = y_{\mathrm{dc},ij} \quad ; \quad \text{with } j \neq i \tag{57}$$

From these second partial derivatives the Hessian matrix can be constructed, which will have a dimension dependent on the number of converters that the studied system has. Each of the elements that appear in the matrix have m x m dimensions, where m is the number of converters in the system. Equation 58 shows the Hessian matrix, where the second derivatives where P_{dc} is involved, which are equal to zero, are displayed directly in the matrix.

$$G_{XX}^{P_{\mathrm{dc}}} = \begin{bmatrix} G_{U_{\mathrm{dc}}U_{\mathrm{dc}}}^{P_{\mathrm{dc}}} & G_{P_{\mathrm{dc}}U_{\mathrm{dc}}}^{P_{\mathrm{dc}}} \\ G_{U_{\mathrm{dc}}P_{\mathrm{dc}}}^{P_{\mathrm{dc}}} & G_{P_{\mathrm{dc}}P_{\mathrm{dc}}}^{P_{\mathrm{dc}}} \end{bmatrix} = \begin{bmatrix} G_{U_{\mathrm{dc}}U_{\mathrm{dc}}}^{P_{\mathrm{dc}}} & 0 \\ 0 & 0 \end{bmatrix} \tag{58}$$

This constraint allows simulating the behavior of the DC system from the definition of the power flow in it, establishing which of the converters inject power to the AC system and which consume power from it. Defining also the losses due to energy transmission in HVDC lines.

5.3.3 Converter losses

The equality constraint related to the converter losses refers to Equation 11 of the section 3.3.2. This constraint explains the relationship between the AC and DC sides of the converter, relating the power flows on both sides from the definition of certain losses. Equation 59 shows this constraint, which depends on the active power on the AC side of the converter ($P_{\mathrm{c},i}$), on the power coming from the DC system ($P_{\mathrm{dc},i}$) and on the losses ($P_{\mathrm{loss},i}$) due to commutation or conduction, among others.

$$G^{\mathrm{Conv}}(X) = P_{\mathrm{c},i} - P_{\mathrm{dc},i} + P_{\mathrm{loss},i} = 0 \tag{59}$$

Developing the loss factor in the converter, it can be regarded in Equation 60 how there is a non-linear dependence with respect to the defined operating variables ($P_{\mathrm{c},i}$, $Q_{\mathrm{c},i}$ and $P_{\mathrm{dc},i}$). With these characteristics, the $G^{\mathrm{Conv}}(X)$ constraint would result in a non-linear equality constraint [16].

$$G^{\mathrm{Conv}}(X) = P_{\mathrm{c},i} - P_{\mathrm{dc},i} + a_i + b_i \cdot \frac{\sqrt{P_{\mathrm{c,i}}^2 + Q_{\mathrm{c,i}}^2}}{U_{\mathrm{c},i}} + c_i \cdot \frac{P_{\mathrm{c,i}}^2 + Q_{\mathrm{c,i}}^2}{U_{\mathrm{c},i}^2} = 0 \tag{60}$$

In order to simplify the model, the loss factor in the converters is taken as negligible. In this way, the constraint $G^{\mathrm{Conv}}(X)$ equals the input and output powers of the converter, converting

it into a linear equality constraint, as shown in Equation 61. The fact of having a linear equality constraint avoids the calculation of the Jacobian and Hessian matrices.

$$G^{\text{Conv}}(X) = P_{\text{c},i} - P_{\text{dc},i} = 0 \tag{61}$$

This constraint allows to directly define the power exchange between AC and DC systems through the converter from a linear equality constraint. It is possible to neglect the loss factor due to the high efficiency of the VSC power converters used.

5.3.4 Power flow in the AC side of the converter

This non-linear equality constraint deals with the definition of the power flow in the AC side of the converter from its dependence on the state variables $U_{\text{c},i}$, $\theta_{\text{c},i}$, $U_{\text{s},i}$, $\theta_{\text{s},i}$, $P_{\text{c},i}$and $Q_{\text{c},i}$. Two power flows are differentiated: $G^{P_{\text{c}}}(X)$ (for calculating active power flow) and $G^{Q_{\text{c}}}(X)$ (for calculating reactive power flow), based on those defined in the section 3.3.3, in Equations 25 and 26. It should be noted that the converter station model used is the one that does not have a filter.

$$G^{P_{\text{c}}}(X) = U_{\text{c},i}^2 \cdot G_{\text{tc},i} - U_{\text{s},i}U_{\text{c},i} \cdot \left[G_{\text{tc},i} \cdot \cos\left(\theta_{\text{s},i} - \theta_{\text{c},i}\right) - B_{\text{tc},i} \cdot \sin\left(\theta_{\text{s},i} - \theta_{\text{c},i}\right)\right] - P_{\text{c},i} = 0 \tag{62}$$

$$G^{Q_{\text{c}}}(X) = -U_{\text{c},i}^2 \cdot B_{\text{tc},i} + U_{\text{s},i}U_{\text{c},i} \cdot \left[G_{\text{tc},i} \cdot \sin\left(\theta_{\text{s},i} - \theta_{\text{c},i}\right) + B_{\text{tc},i} \cdot \cos\left(\theta_{\text{s},i} - \theta_{\text{c},i}\right)\right] - Q_{\text{c},i} = 0 \tag{63}$$

The constraints about the calculation of the active and reactive power on the AC side of the converter can be grouped to show the calculation of the power in a complex way, as apparent power. The way in which $G^{S_{\text{c}}}$ is determined is the one shown in Equation 64.

$$G^{S_{\text{c}}} = [\, G^{P_{\text{c}}} \,] + j \cdot [\, G^{Q_{\text{c}}} \,] \tag{64}$$

To simplify the nomenclature used to define the first partial derivatives of the constraint $G^{S_{\text{c}}}(X)$, Equation 65 shows the equivalence of these derivatives as a function of the variable X. This variable X can take the value of any of the state variables that define the constraint. All the first partial derivatives used for the definition of the Jacobian matrix of the constraint $G^{S_{\text{c}}}(X)$ are presented in Appendix 1.2, showing the first derivatives for active ($G_X^{P_{\text{c}}}$) and reactive ($G_X^{Q_{\text{c}}}$) power separately.

$$G_X^{S_{\text{c}}} = \frac{\partial G^{S_{\text{c}}}}{\partial X} \tag{65}$$

With the first partial derivatives defined, it can be constructed the Jacobian matrix. In this case, the matrix will have dimensions m x n, where the number of rows m is equal to the number of converters that the studied system has, and with a total of n columns equivalent to the number of state variables that the constraint has (in this case six). Equation 66 shows the Jacobian matrix.

$$G_X^{S_c} = \begin{bmatrix} G_{U_c}^{S_c} & G_{U_s}^{S_c} & G_{\theta_c}^{S_c} & G_{\theta_s}^{S_c} & G_{P_c}^{S_c} & G_{Q_c}^{S_c} \end{bmatrix} \tag{66}$$

Equation 67 shows the simplified nomenclature referring to the second partial derivatives. All the second partial derivatives used for the definition of the Hessian matrix are shown in Appendix 1.2, again showing the derivatives for active ($G_{XX}^{P_c}$) and reactive ($G_{XX}^{Q_c}$) power separately. It should be noted that all second derivatives where P_c or Q_c are involved are equal to zero.

$$G_{XX}^{S_c} = \frac{\partial G_X^{S_c}}{\partial X} \tag{67}$$

From here, the Hessian matrix can be defined as shown in Equation 68. The dimensions of the Hessian matrix depend on the number of AC nodes and the number of converters that the studied system has. In this way, the dimension of each of the variables determines the size of the matrix. For example, for a system with 10 AC nodes and 3 converters, the dimensions of the element $G_{U_sU_c}^{S_c}(\lambda)$ are 10x3 (10 values of U_s and 3 values of U_c), while the size of the Hessian matrix is 32x32. It should be noted that for the definition of the Hessian matrix, all the elements are dependent on the Lagrangian multiplier λ.

$$G_{XX}^{S_c} = \begin{bmatrix} G_{U_cU_c}^{S_c}(\lambda) & G_{U_sU_c}^{S_c}(\lambda) & G_{\theta_cU_c}^{S_c}(\lambda) & G_{\theta_sU_c}^{S_c}(\lambda) & G_{P_cU_c}^{S_c}(\lambda) & G_{Q_cU_c}^{S_c}(\lambda) \\ G_{U_cU_s}^{S_c}(\lambda) & G_{U_sU_s}^{S_c}(\lambda) & G_{\theta_cU_s}^{S_c}(\lambda) & G_{\theta_sU_s}^{S_c}(\lambda) & G_{P_cU_s}^{S_c}(\lambda) & G_{Q_cU_s}^{S_c}(\lambda) \\ G_{U_c\theta_c}^{S_c}(\lambda) & G_{U_s\theta_c}^{S_c}(\lambda) & G_{\theta_c\theta_c}^{S_c}(\lambda) & G_{\theta_s\theta_c}^{S_c}(\lambda) & G_{P_c\theta_c}^{S_c}(\lambda) & G_{Q_c\theta_c}^{S_c}(\lambda) \\ G_{U_c\theta_s}^{S_c}(\lambda) & G_{U_s\theta_s}^{S_c}(\lambda) & G_{\theta_c\theta_s}^{S_c}(\lambda) & G_{\theta_s\theta_s}^{S_c}(\lambda) & G_{P_c\theta_s}^{S_c}(\lambda) & G_{Q_c\theta_s}^{S_c}(\lambda) \\ G_{U_cP_c}^{S_c}(\lambda) & G_{U_sP_c}^{S_c}(\lambda) & G_{\theta_cP_c}^{S_c}(\lambda) & G_{\theta_sP_c}^{S_c}(\lambda) & G_{P_cP_c}^{S_c}(\lambda) & G_{Q_cP_c}^{S_c}(\lambda) \\ G_{U_cQ_c}^{S_c}(\lambda) & G_{U_sQ_c}^{S_c}(\lambda) & G_{\theta_cQ_c}^{S_c}(\lambda) & G_{\theta_sQ_c}^{S_c}(\lambda) & G_{P_cQ_c}^{S_c}(\lambda) & G_{Q_cQ_c}^{S_c}(\lambda) \end{bmatrix} \tag{68}$$

With the definition of the constraint about the active and reactive power on the AC side of the converter, all the operation constraints around the modelling of the DC system and the converter station have already been developed, in the absence of defining the converter control system.

5.3.5 Control of the converters

The last equality constraints to be defined are the control constraints, which will allow the optimization model to simulate the behavior of the converters control system. The control constraints are based on Equations 27-30 from section 3.3.4, where the state variables ($U_{\mathrm{dc},i}$, $U_{\mathrm{s},i}$, $P_{\mathrm{s},i}$ and $Q_{\mathrm{s},i}$) are equated with the control variables ($U_{\mathrm{dc},i}^{\mathrm{Ref}}$, $U_{\mathrm{s},i}^{\mathrm{Ref}}$, $P_{\mathrm{s},i}^{\mathrm{Ref}}$ and $Q_{\mathrm{s},i}^{\mathrm{Ref}}$). They are made up of two types of constraints that difference the control channels to be controlled: the active channel ($G^{\mathrm{Active}}(X)$) and the reactive channel ($G^{\mathrm{Reactive}}(X)$). Each of the converters will try to control voltage or power parameters depending on whether it is a master or slave converter, respectively.

In the case of master converters, these constraints will try to control the voltage on both sides of the converter. Equations 69 and 70 present these linear control constraints for the active and reactive channel.

$$G^{\mathrm{Active}}(X) = U_{\mathrm{dc},i} - U_{\mathrm{dc},i}^{\mathrm{Ref}} \;\; ; \quad \text{for Master Converter} \tag{69}$$

$$G^{\mathrm{Reactive}}(X) = U_{\mathrm{s},i} - U_{\mathrm{s},i}^{\mathrm{Ref}} \;\; ; \quad \text{for Master Converter} \tag{70}$$

In the same way, Equations 71 and 72 refer to the linear constraints applied to slave converters in order to control the active and reactive power supplied through their active and reactive channels.

$$G^{\mathrm{Active}}(X) = P_{\mathrm{s},i} - P_{\mathrm{s},i}^{\mathrm{Ref}} \;\; ; \quad \text{for Slave Converter} \tag{71}$$

$$G^{\mathrm{Reactive}}(X) = Q_{\mathrm{s},i} - Q_{\mathrm{s},i}^{\mathrm{Ref}} \;\; ; \quad \text{for Slave Converter} \tag{72}$$

There will be a total number of control constraints equal to twice the number of converters available in the studied system, since for each converter, as mentioned, there will be a constraint for the active channel and another for the reactive channel.

5.4 Inequality constraints

This section presents the inequality constraints that are part of the OPF model for AC/DC hybrid networks. From the OPF model for AC systems, the non-linear inequality constraint referred to the branch flow limits in the AC transmission lines, the limitations in the active and reactive power generated and the bounds for the voltage at AC nodes must be taken into account. In addition, all those inequality constraints that define the converter limits, the grid code and the bounds for all the state and control variables must be added to the formulation.

5.4.1 Converter limits

In order to ensure the correct operation of the VSC converters, certain electrical parameters must be limited so that the steady state operating point fulfill the PQ capacity limit [24, 25]. In this way, the operating area of the VSC converters will see their current levels and voltages (both on the AC and DC sides) and the active and reactive power injected into the AC system limited. Figure 5.1 shows an example of PQ capacity diagram [25, 26], where all the limitations are taken into account and the converter operating area is shown in green.

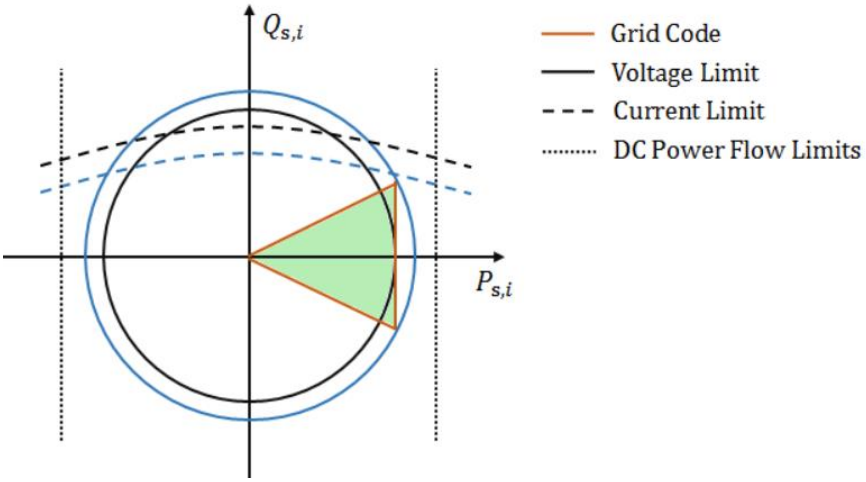

Figure 5.1: Example of PQ capacity diagram of a VSC converter station.

For the OPF model, the voltage on the DC side of the converter, the voltage in the AC nodes and the active and reactive power injected into the AC system by the converters are limited from the definition of their bounds, since they are treated as state variables, so they are defined in the section 5.4.2. On the other hand, some inequality constraints are needed for the current limits.

Equation 73 shows the inequality constraint that limits the level of current flowing through the DC system, thus respecting the electrical limits of the HVDC cables.

$$H^{\mathrm{I_{dc}}}(X) = \left(I_{\mathrm{dc},i}\right)^2 - (I_{\mathrm{dc}}^{\max})^2 \leq 0 \tag{73}$$

In the same way, Equation 74 represents the inequality constraint in charge of limiting the current that flows on the AC side of the converter. With this limitation, it is intended not to exceed the maximum current admitted by the IGBT transistors.

$$H^{\mathrm{I_c}}(X) = \left(I_{\mathrm{c},i}\right)^2 - (I_{\mathrm{c}}^{\max})^2 \leq 0 \tag{74}$$

It should be noted that in the converter stations the power flows are taken as bidirectional, since the converters can operate as rectifiers or inverters indistinctly. For this reason, only one maximum current value is defined, which is valid for both directions.

5.4.2 State variables' bounds

In this section, the bounds for all the state variables that are added in the OPF model applied to AC/DC hybrid networks will be defined as in [14]. In MatPower [4], these bounds are not presented as inequality constraint, but a maximum and a minimum value is given for each of the variables by its own definition. The state variables for which bounds are imposed are all those that make up the vector x^{T} presented in Equation 36. Equation 75 presents the mathematical formulation for these bounds in a general way for all state variables.

$$X_i^{\mathrm{Min}} \leq X_i \leq X_i^{\mathrm{Max}} \tag{75}$$

Where X_i represents each of the state variables collected in the vector of optimization variables x^{T} and for each node i, and X_i^{Min} and X_i^{Max} refer to the predefined minimum and maximum values for each of the variables. Note that each of the added state variables $(P_{\mathrm{s},i}, Q_{\mathrm{s},i}, P_{\mathrm{c},i}, Q_{\mathrm{c},i}, P_{\mathrm{dc},i}, U_{\mathrm{c},i}, \theta_{\mathrm{c},i}, U_{\mathrm{dc},i}, U_{\mathrm{dc},i}^{\mathrm{Ref}}, P_{\mathrm{s},i}^{\mathrm{Ref}}, Q_{\mathrm{s},i}^{\mathrm{Ref}}, U_{\mathrm{s},i}^{\mathrm{Ref}})$ will be made up of a total number of values equivalent to the number of converters that the studied system has. On the other hand, each of the state variables already existing in the OPF model for AC systems $(U_i, \theta_i, P_{\mathrm{G},i}, Q_{\mathrm{G},i})$ have a total number of values equal to the number of AC nodes that the network has.

With all this, and once the objective function, the state variables with their respective bounds and all the constraints (both equality and inequality constraints) are defined, the extended formulation for the OPF model applied to AC/DC hybrid grids is completely given.

6 Proposed test system

The test system that is introduced in this section corresponds to the hybrid AC/DC transmission power system for which the optimal power flow study is carried out, based on the model proposed in the previous sections. It is a test system based on the one developed in article [27], not only the structure and generation and consumption data are offered, but also the technical data of interest on the transmission lines, VSC converters and network limits; all of them are necessary to perform the OPF calculation.

6.1 AC system

The AC system has a total of 66 AC nodes, which are divided into three control areas. The three areas are interconnected with each other with five transmission lines. About the generation units and the loads, they are directly connected to the system. There are a total of 17 synchronous generation units and two large-scale wind farms.

Figure 6.1 shows the structure of the AC system, which locates the synchronous generation units, the wind farms and the converter stations; in addition to showing the different transmission lines that interconnect the AC nodes.

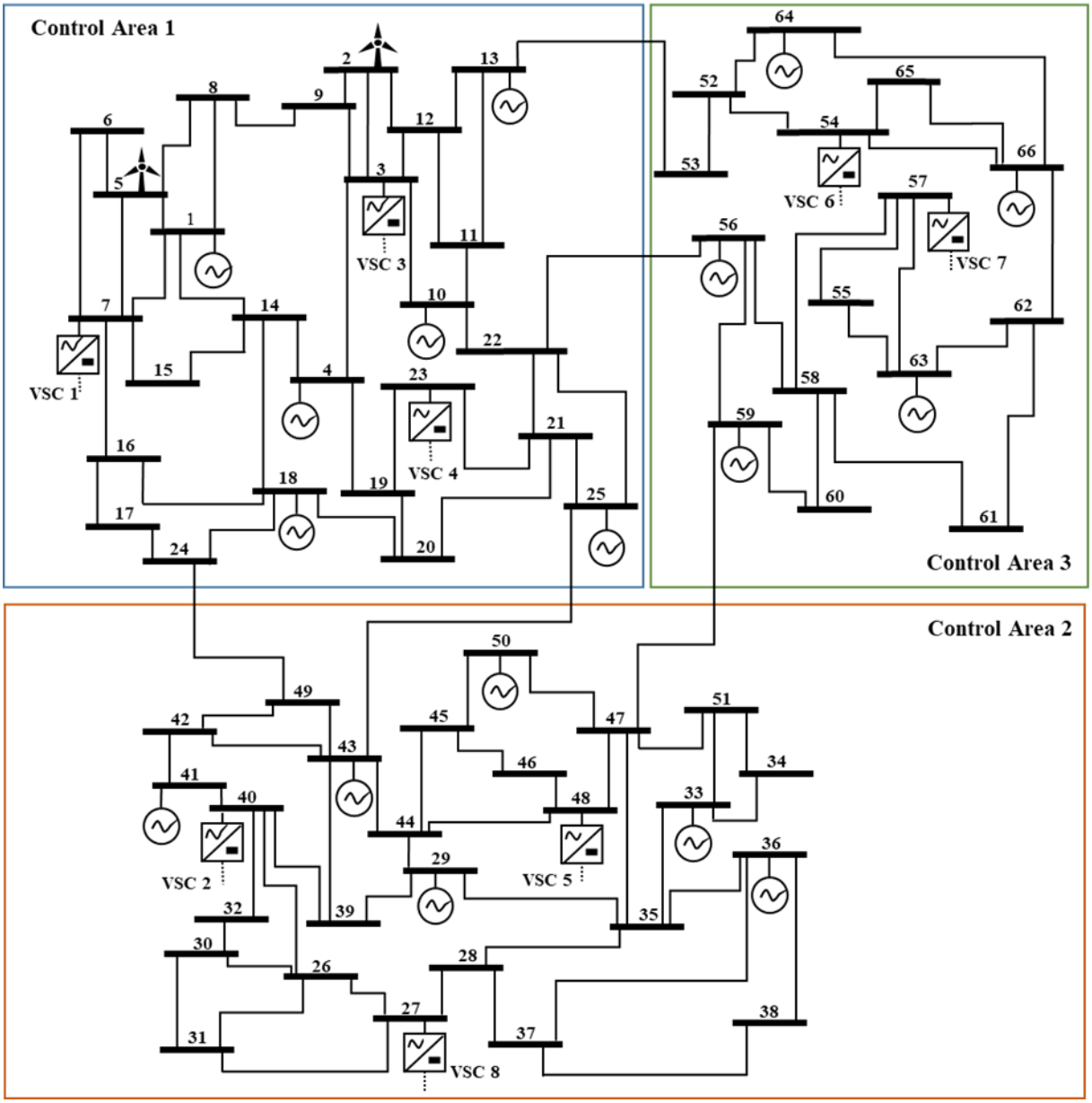

Figure 6.1: AC system with generation units, wind farms, VSCs and transmission lines.

The AC system has a total of 102 AC branches, each with a thermal current limit of 3500 A. It is also important to point out that the transformers will not be taken into account in the analysed system, since they are not necessary to perform the OPF calculations. According to the defined AC system model, all branches will have an equivalent resistance and reactance as is shown in Table 6.1, which includes these characteristics for a standard 400 kV OHL. Each of the AC transmission lines is 100 km long.

Table 6.1: Data for 400 kV OHL (Al/St 240/40).

R' (Ω/km)	X' (Ω/km)	C' (nF/km)	I_c^{Max} (A)
0.03	0.26	13.5	3500

In the original system presented in article [27], there is an offshore wind farm that is located outside the commented control areas and that allows the system having another generation point, with one more AC node (node 67). However, the offshore wind farm will not be taken into account in this work, as it focuses only on the OPF calculation for hybrid AC/DC transmission with embedded DC-grids.

6.2 HVDC system

The HVDC system has a total of 8 VSC converter stations that allow it to be connected to the AC system discussed in the previous section 6.1. This system will have a bipolar operation and will work at ±500 kV. In the original system of article [27] there is a ninth VSC converter station that allows the offshore wind farm to be linked to the system by means of a single tap line, but this will not be taken into account as previously mentioned.

The OPF study is carried out for three different structures of the HVDC system. Each of these structures will correspond to a different stage of development of the meshed HVDC system, since its construction is intended to be carried out in a staggered manner. In this way, the results of the OPF are shown for the different stages of implementation of the HVDC system.

Stage 1 consists of a set of three independent point-to-point interconnections. This system has a total of 7 VSC converter stations and only 4 HVDC branches. Figure 6.2 shows the structure of the HVDC system in stage 1.

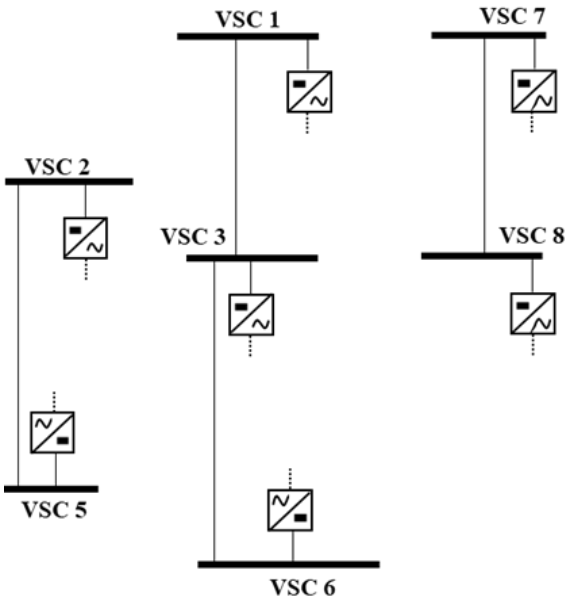

Figure 6.2: HVDC system for stage 1.

In order to obtain a partially meshed system, in stage 2 some interconnections are made between the three subsystems presented in stage 1. In addition, one more VSC converter station is added that allows offering a more robust HVDC system and expanding its dimensions. With this, there are a total of 8 VSC converter stations and 8 HVDC branches. The structure of the HVDC system in stage 2 is presented in Figure 6.3.

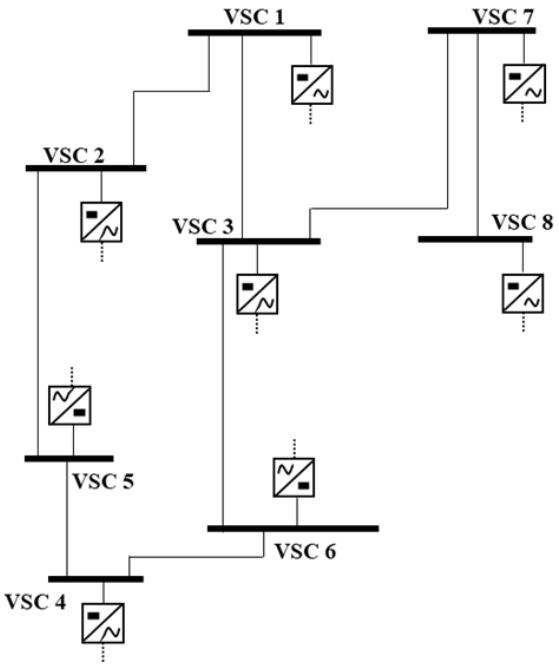

Figure 6.3: HVDC system for stage 2.

Finally, for stage 3 there is a fully meshed HVDC system, in which there is no tap line. The stage 3 HVDC system has a total of 8 VSC converter stations and 10 HVDC transmission lines, arranged as shown in the Figure 6.4.

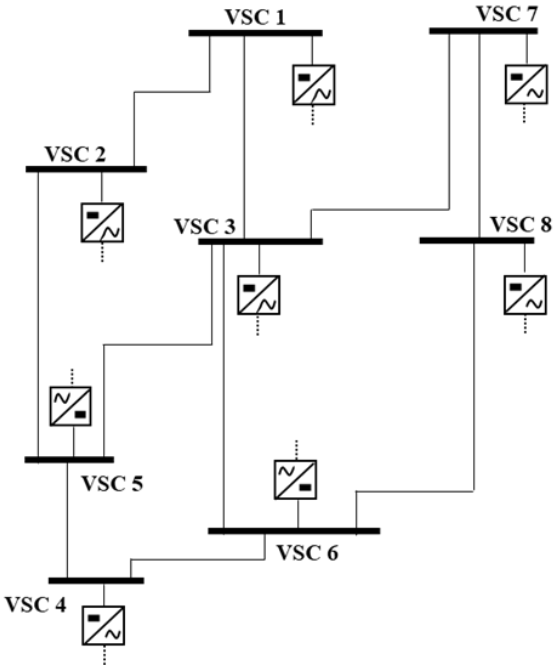

Figure 6.4: HVDC system for stage 3.

All transmission lines in the HVDC system are modelled as cables. The technical data related to the equivalent resistance and capacity of the cabling are presented in Table 6.2. The data for ±400 kV cables are taken as acceptable, since there is no data available for the ±500 kV that the system has. Comment that the transmission capacity of the lines is set as 3500 A, which is equivalent to 3500 MVA for bipolar operation at ±500 kV. Each of the HVDC branches will have a total length of 300 km.

Table 6.2: Data for ±400 kV HVDC cable.

R' (Ω/km)	C' (μF/km)	I_c^{Max} (A)
0.01	0.01	3500

6.3 Input data

The input data related to the considered test system are tabulated in Appendix 2, following the structure and nomenclature specified in the MatPower 7.0 manual [4]. They are organized in different tables, each one related to one of the input data matrices that the user can define in the modified version of MatPower for the calculation of the OPF in hybrid AC/DC networks. These matrices are related to the input data for AC nodes, generation units, AC transmission lines, VSC converters and HVDC transmission lines.

As input data for each of the AC nodes: the type of bus (PQ, PV or Slack), the demand for active and reactive power (in MW and Mvar), the initial value of the voltage magnitude (in pu) and the voltage angle (°) and the maximum and minimum value allowed for this bus voltage in pu. In addition, the area of which each node is part of the three presented is specified; as well as the base voltage, which in all cases is 380 kV. It should be noted that the shunt conductance and susceptance are considered null. These data are presented in Appendix 2.1.

For synchronous generation units is offered the bus to which they are connected, the initial value of active and reactive power generated (in MW and Mvar) and the voltage magnitude set point (in pu). It also shows the maximum and minimum value of active and reactive generation power (in MW and Mvar) and the base power value (in MVA) for each generation unit. These data are presented in Appendix 2.2.

The matrix relative to the branch data shows the origin and destination bus for each transmission line, the equivalent resistance and impedance of the line in pu and the long term rating that allows specifying the branch flow limits. These data are presented in Appendix 2.3.

On the input data for each VSC converter station, the AC bus to which it is connected is offered, as well as the initial value for the active and reactive power injected into the respective AC bus (in MW and Mvar), the magnitude and the angle for the voltage on the AC side of the converter in pu and the voltage on the DC side of the converter in pu. The maximum and minimum values are also defined for the power injected into the AC bus and for the different variable voltages in pu. Furthermore, it is specified if it is a master or a slave converter station, applied to its control. These data are presented in Appendix 2.4.

Finally, for the definition of the input data related to the HVDC transmission lines, the origin and destination buses of each branch, the equivalent resistance in pu and the transmission capacity of the line in amperes are offered. These data are presented in Appendix 2.5. The base value of the equivalent resistance of the HVDC line has been calculated from Equation 76, for

which a 500 kV base voltage in DC and a 100 MW base power for a bipolar HVDC line have been considered.

$$R_{\mathrm{dc,base}} = \frac{U_{\mathrm{dc,base}}^2}{P_{\mathrm{dc,base}}} \tag{76}$$

The initial values presented for the different variables of the OPF model of the AC/DC system have been determined from a steady state study based on a power flow calculation. From this, it has been possible to extract the initial data of the AC bus voltage, of the generated and injected active and reactive power from the generation units and the VSC converter stations respectively, and the voltage magnitude set points also from the generators and the converters.

7 Optimal power flow results

From the MatPower extension for the calculation of the OPF for hybrid AC/DC grids, the results for the different stages of the test system presented in section 6 are shown.

7.1 Test system results I – Stage comparison

This section presents a comparison of the OPF results obtained for the different stages of the test system. A comparison with the initial values defined in the input data matrices is also shown for some of the results, in order to check how the model has varied these values to obtain an optimal operation of the system.

First, the total losses in the test system for each stage are presented in Figure 7.1. As can be seen, the stage with the most losses is stage 1. This is due to the fact that it is the stage that has an HVDC system with the lowest level of meshing (based on three independent point-to-point interconnections), and which performs less use of this HVDC system. On the other hand, the one with the lowest losses is stage 3, which has a fully meshed HVDC system.

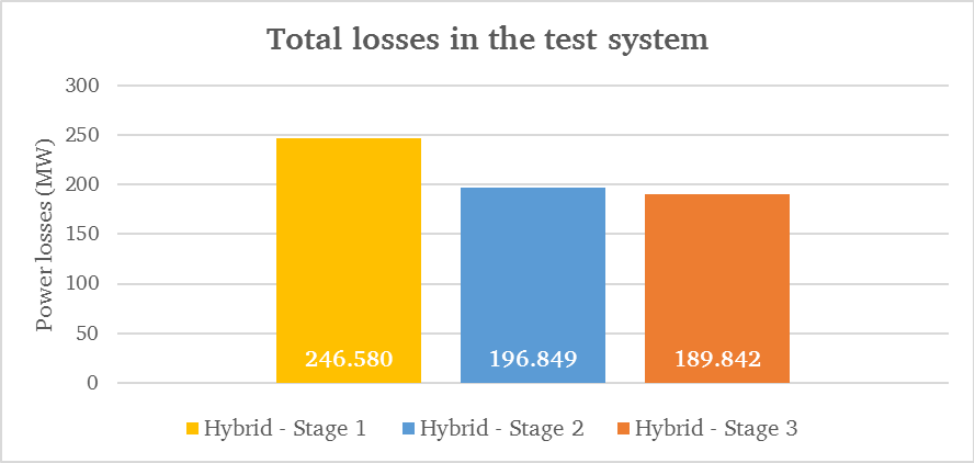

Figure 7.1: OPF total losses for each stage.

Table 7.1 depicts the losses in depth for the different stages. This table differentiates the losses in AC and HVDC systems, and shows the relative losses with respect to the generation in each case.

Table 7.1: OPF total losses and generation for each stage.

Total losses and generation					
	Generation (MW)	**AC losses (MW)**	**DC losses (MW)**	**Losses (MW)**	**% losses**
Hybrid - Stage 1	9517.68	246.58	4.55	251.13	2.64%
Hybrid - Stage 2	9475.49	196.85	11.64	208.49	2.20%
Hybrid - Stage 3	9462.30	189.84	5.91	195.75	2.07%

As previously mentioned, stage 1 is the one with the highest losses in the AC system and the lowest losses in the DC system. This is due to the little power transmission through its HVDC lines. The difference in the losses of the HVDC system for stages 2 and 3 is explained by the different levels of meshing they have. In stage 2, some of the HVDC lines transmit very high powers, which leads to higher losses, due to the quadratic dependence of the voltage on the losses in DC. On the other hand, stage 3 has a much more balanced HVDC system, which, despite transmitting similar amounts of power, is capable of distributing it among all its lines.

Figure 7.2 presents the power generated by each of the test system generators (G). The generation for the three stages and the initial values are shown.

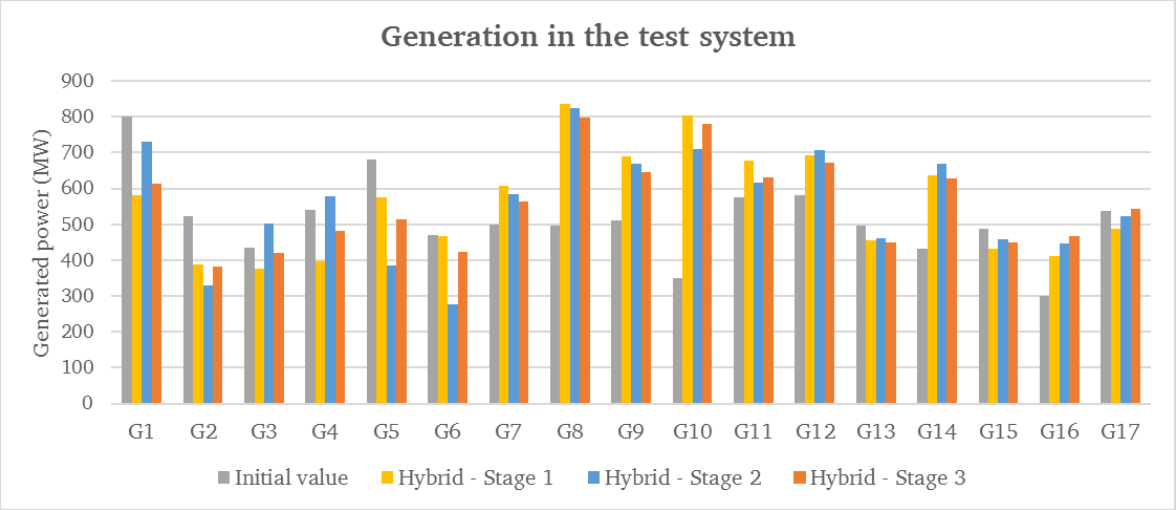

Figure 7.2: OPF generation for each stage and initial values.

The power generated in each of the generators has been optimized, within its bounds, to have to transmit the least power over long distances, in order to minimize transmission losses. As can be seen, the generation has been varied with respect to the initial value in all the stages. The G1 (slack bus) generation has been reduced in the three stages with respect to its initial value.

Figure 7.3 shows the AC bus voltage of the test system for each of the AC nodes (B), and for all the stages and initial values.

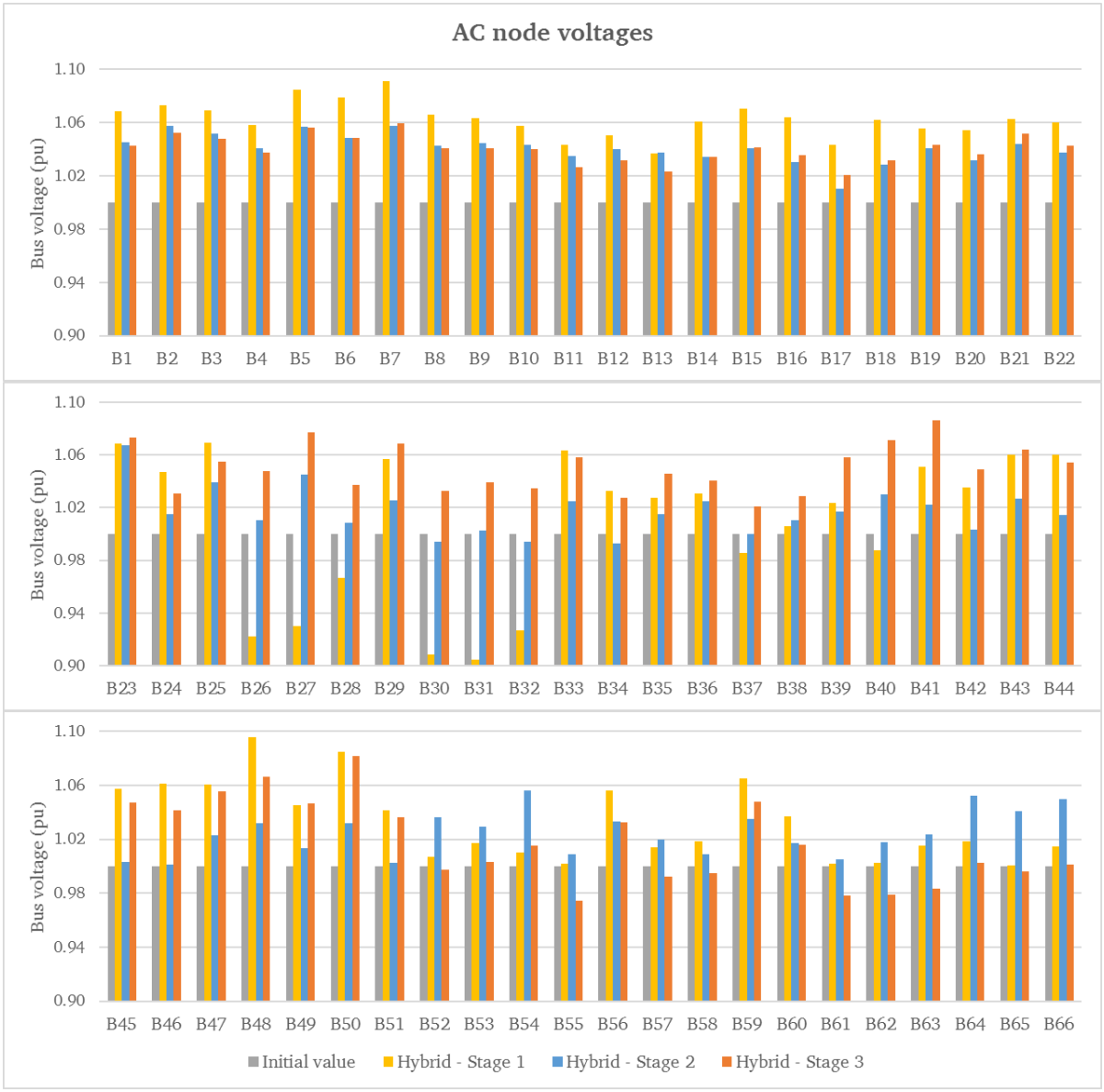

Figure 7.3: OPF AC node voltages for each stage and initial values.

The voltage levels for each of the AC buses are within the defined bounds (between 0.9 and 1.1). Some of the nodes have voltage values very close to the lower limit. This is due to the fact that these buses are further away from generation and converters, and are also connected to loads with higher active and reactive power demand. While the buses with voltages closer to the upper limit are connected with generators or converters.

Figure 7.4 shows the power injected into the AC system from each of the converters. This power is positive when the converter injects it into the AC system and is negative when the converter injects it into the DC system. The results for the three stages and the initial values are presented.

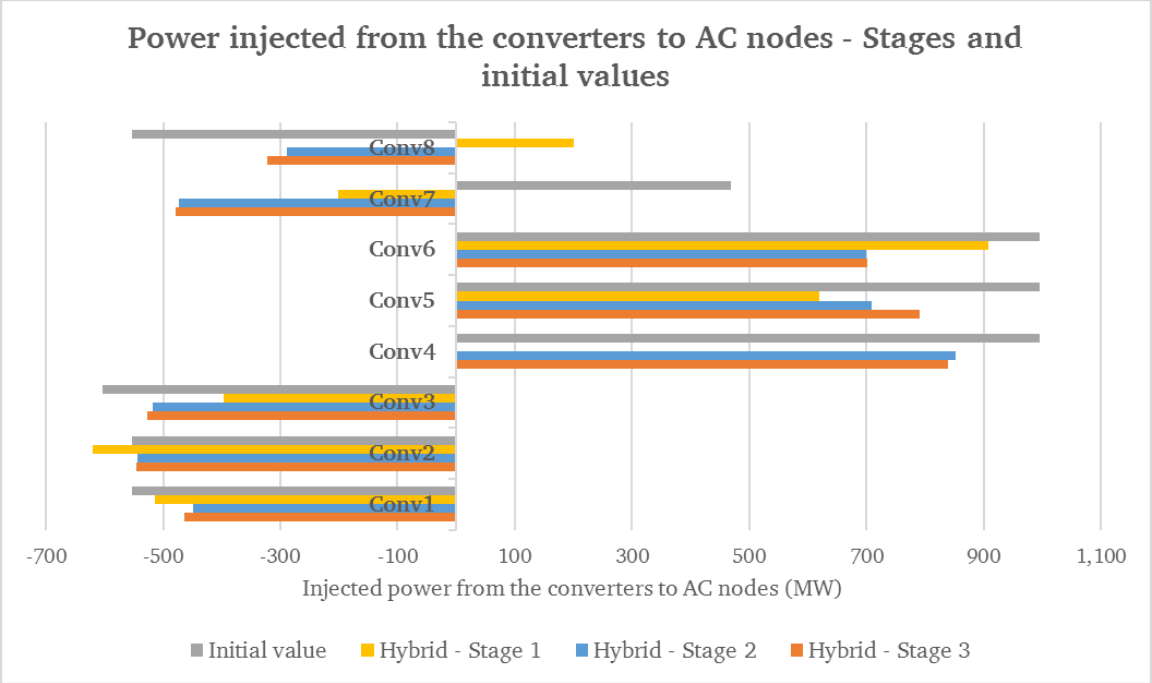

Figure 7.4: OPF injected power from converters to AC nodes for each stage and initial values.

Again, the results obtained for the stages differ from the initial values, since the optimal results are taken for each of the stages. It should be noted that, in stage 1, converter 4 has no injected power, because this converter is not connected to the system in this stage. It is interesting to see that converter 7 has changed its power direction for all the stages with respect to the initial value. This is due to the fact that converter 7 is close to several generators, and the OPF calculation optimizes the power flow from converter 7 to other converters in areas with higher energy need.

7.2 Test system results II - Optimal solution

In this section, a comparison of the total losses of the system for different scenarios is presented for each of the stages. The first scenario always corresponds to the OPF, while for the rest of the scenarios the losses are defined from the PF calculation with different conditions. The variations considered for each scenario in the PF calculation apply to the active power generated by each generator (except for the slack bus), to the power transmitted by the converters and to

the selection of the master converter. The bounds defined for each parameter have always been respected.

Figure 7.5 presents the losses in the test system with stage 1 for different scenarios. It should be remembered that stage 3 has three independent point-to-point interconnections, so a master converter has to be defined for each of the interconnections.

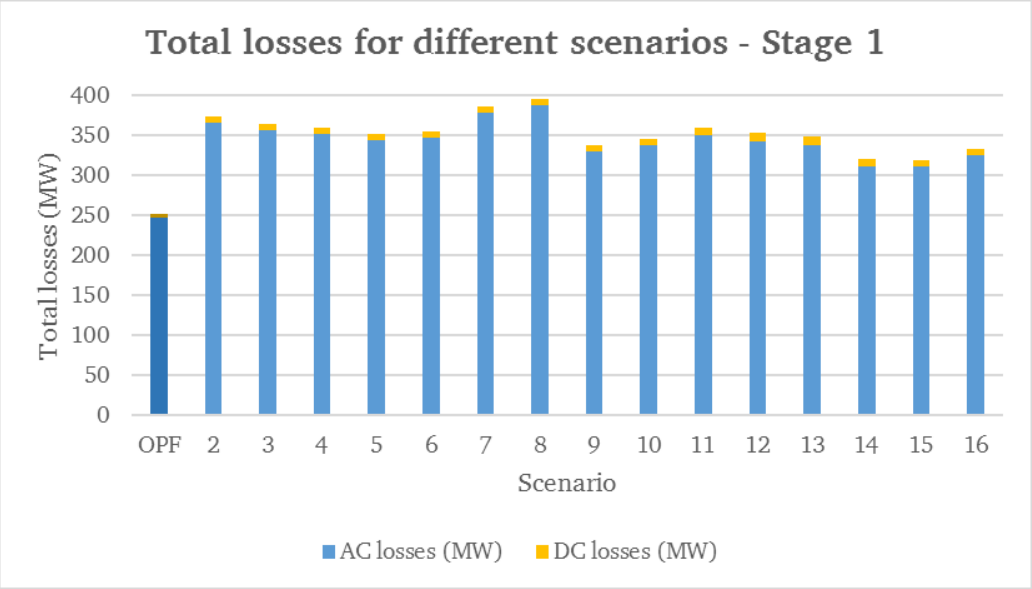

Figure 7.5: Total losses for different scenarios for stage 1.

For the test system with stage 2, Figure 7.6 shows the losses obtained for different scenarios. In the same way as Figure 7.7 for the test system with stage 3.

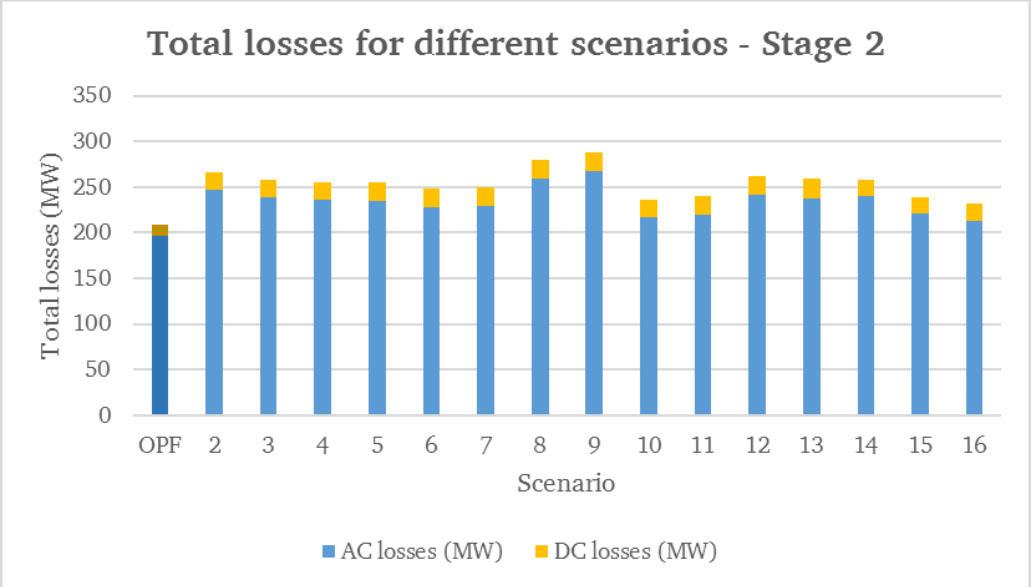

Figure 7.6: Total losses for different scenarios for stage 2.

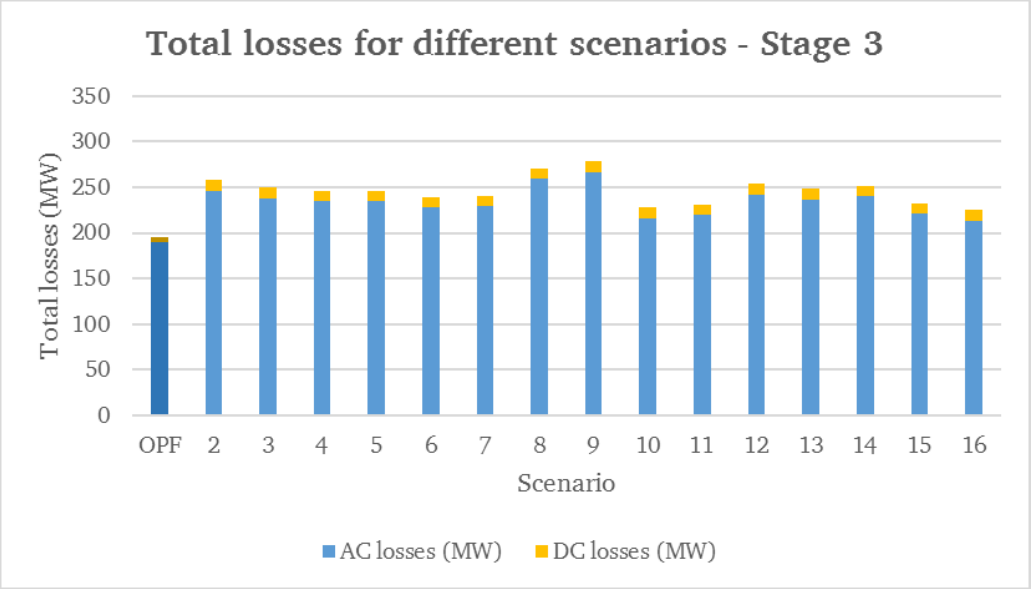

Figure 7.7: Total losses for different scenarios for stage 3.

For all stages, the lowest losses are presented in the scenario defined through the OPF. With this, the correct operation of the MatPower extension on OPF calculation applied to hybrid AC/DC grids is demonstrated. Note that the PF calculations have been made from MatACDC [28], a Matlab based open source program for AC/DC power flow analysis.

7.3 Case 5 results

Additionally, the analysis of a second test system based on Case 5 of MatACDC [28] is presented. In order to demonstrate the generality of the developed MatPower extension, it has been used another hybrid test-bench system. Case 5 is made up of 5 AC nodes, 7 AC lines, 2 generators, 3 converters and 3 HVDC lines.

In the same way as in the previous section, the system losses for different scenarios are presented. The first scenario is based on the OPF, while the other scenarios will be defined from the PF calculation with different conditions. Each of the scenarios defined by the PF will have a variation in the power generated by the generators (except for the slack bus). Figure 7.8 shows the comparison of the losses for the different scenarios.

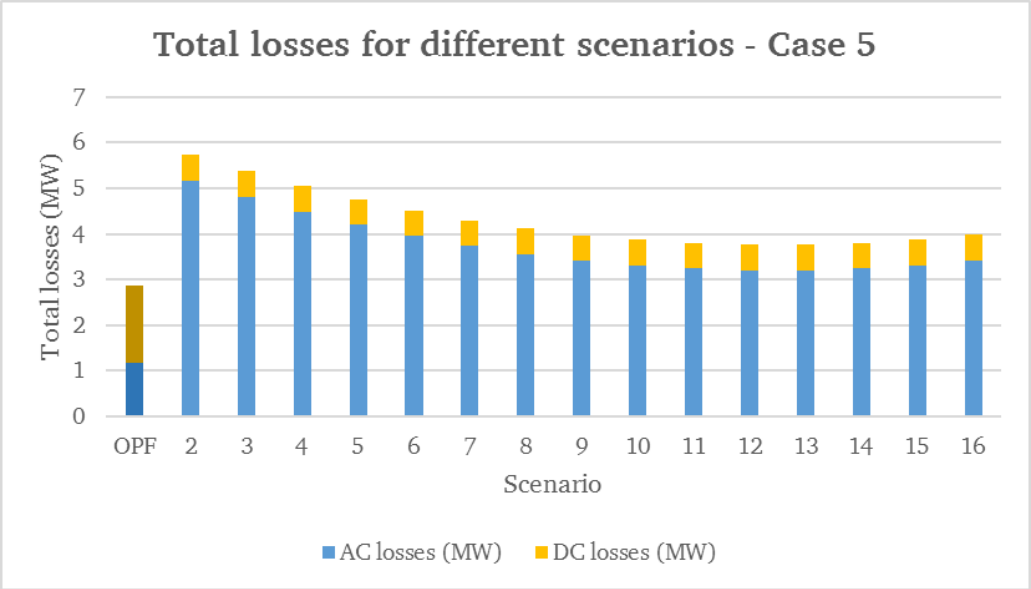

Figure 7.8: Total losses for different scenarios for Case 5.

As can be seen, the OPF scenario is the one that shows the least losses. In this case, making greater use of the HVDC transmission system has been taken as the optimal option, which has made possible to considerably reduce AC transmission losses.

8 Conclusions

The purpose of this thesis was the development of an extension of MatPower that would allow the calculation of the optimal power flow applied to hybrid AC/DC grids. From this extension, it was intended to determine the impact of the DC system on a specific test system. To achieve these objectives, the physical modeling of hybrid grids has first been presented. An OPF model based on this modeling has been defined in order to minimize system losses, whose new variables and constraints have been introduced. The MatPower extension has been developed, applying the theoretical OPF model defined for hybrid grids to the existing one for AC networks. Finally, the results that demonstrate the correct operation of the extension have been presented, and the results obtained for the studied test system have been analyzed.

From the results of the studied test system, it can be ensured that the incorporation of an HVDC system reduces the global losses of the system. In addition, from the analysis of the different stages, it has been seen that the most efficient stage is the one with a fully meshed HVDC system.

The difficulties that have appeared during the realization of the project have been mainly related to the development of the MatPower extension. This is due to the complexity of the MatPower base code, which has had to be modified to incorporate the new variables and constraints. The need to work with Jacobian and Hessian matrices has also been a difficulty, which has been the hardest mathematical complication of the thesis.

In future works an improvement of the MatPower extension may be made. Some of the simplifications presented can be cancelled, through the development of new constraints. In addition, the improvement of the bounds for the variables with the application of penalties would allow the results to be even closer to realistic values.

Appendix

Appendix 1: Constraints' derivatives

In this section of the appendix, the first partial derivatives that make up the Jacobian matrix and the second partial derivatives that complete the Hessian matrix for the constraints related to the nodal power balance (Appendix 1.1) and to the power flow in the AC side of the converter (Appendix 1.2) are presented. In the case of the partial derivatives of the nodal power balance constraint, only those that are not null are shown.

Appendix 1.1: Nodal power balance

First Derivatives

$$\frac{\partial G^{\mathrm{S}}}{\partial \theta} = j\,[V] \cdot \left(\left[I^{\mathrm{bus}^*}\right] - (Y_{\mathrm{busAC}})^* \cdot [V^*]\right) \tag{A1}$$

$$\frac{\partial G^{\mathrm{S}}}{\partial V} = [V] \cdot \left(\left[I^{\mathrm{bus}^*}\right] + (Y_{\mathrm{busAC}})^* \cdot [V^*]\right) \cdot [V]^{-1} \tag{A2}$$

$$\frac{\partial G^{\mathrm{S}}}{\partial P_{\mathrm{G}}} = -C_{\mathrm{G}} \tag{A3}$$

$$\frac{\partial G^{\mathrm{S}}}{\partial Q_{\mathrm{G}}} = -j \cdot C_{\mathrm{G}} \tag{A4}$$

$$\frac{\partial G^{\mathrm{S}}}{\partial P_{\mathrm{s}}} = C_{\mathrm{s}} \tag{A5}$$

$$\frac{\partial G^{\mathrm{S}}}{\partial Q_{\mathrm{s}}} = j \cdot C_{\mathrm{s}} \tag{A6}$$

Second Derivatives

$$\frac{\partial G^{\mathrm{S}}}{\partial \theta^2} = [V^*] \cdot \{(Y_{\mathrm{busAC}})^{*\mathrm{T}} \cdot [V] - (Y_{\mathrm{busAC}})^{*\mathrm{T}} \cdot [V]\} + [V] \cdot \{(Y_{\mathrm{busAC}})^* \cdot [V^*] - [I^{\mathrm{bus}^*}]\} \tag{A7}$$

$$\frac{\partial G^{\mathrm{S}}}{\partial \theta \partial V} = j \cdot [V]^{-1} \cdot \left\{[V^*] \cdot \left((Y_{\mathrm{busAC}})^* \cdot [V] - (Y_{\mathrm{busAC}})^{*\mathrm{T}} \cdot [V]\right)\right\} - [V] \cdot \{(Y_{\mathrm{busAC}})^* \cdot [V^*] - [I^{\mathrm{bus}^*}]\} \tag{A8}$$

$$\frac{\partial G^{\mathrm{S}}}{\partial V^2} = [V]^{-1} \cdot \{[V] \cdot (Y_{\mathrm{busAC}})^* \cdot [V^*] + [V^*] \cdot (Y_{\mathrm{busAC}})^{*\mathrm{T}} \cdot [V]\} \cdot [V]^{-1} \tag{A9}$$

$$\frac{\partial G^{\mathrm{S}}}{\partial V \partial \theta} = j \cdot [V]^{-1} \cdot \left\{[V^*] \cdot \left((Y_{\mathrm{busAC}})^* \cdot [V] - (Y_{\mathrm{busAC}})^{*\mathrm{T}} \cdot [V]\right)\right\} - [V] \cdot \{(Y_{\mathrm{busAC}})^* \cdot [V^*] - [I^{\mathrm{bus}^*}]\} \tag{A10}$$

Appendix 1.2: Power flow in the AC side of the converter

First Derivatives – Active power

$$\frac{\partial G^{P_c}}{\partial U_c} = 2 \cdot U_{c,i} \cdot G_{tc} - U_{s,i} \cdot [G_{tc} \cdot \cos(\theta_{s,i} - \theta_{c,i}) - B_{tc} \cdot \sin(\theta_{s,i} - \theta_{c,i})] \quad \text{(A11)}$$

$$\frac{\partial G^{P_c}}{\partial U_s} = -U_{c,i} \cdot [G_{tc} \cdot \cos(\theta_{s,i} - \theta_{c,i}) - B_{tc} \cdot \sin(\theta_{s,i} - \theta_{c,i})] \quad \text{(A12)}$$

$$\frac{\partial G^{P_c}}{\partial \theta_c} = -U_{c,i} \cdot U_{s,i} \cdot [G_{tc} \cdot \sin(\theta_{s,i} - \theta_{c,i}) + B_{tc} \cdot \cos(\theta_{s,i} - \theta_{c,i})] \quad \text{(A13)}$$

$$\frac{\partial G^{P_c}}{\partial \theta_s} = -U_{c,i} \cdot U_{s,i} \cdot [-G_{tc} \cdot \sin(\theta_{s,i} - \theta_{c,i}) - B_{tc} \cdot \cos(\theta_{s,i} - \theta_{c,i})] \quad \text{(A14)}$$

$$\frac{\partial G^{P_c}}{\partial P_c} = -1 \quad \text{(A15)}$$

$$\frac{\partial G^{P_c}}{\partial Q_c} = 0 \quad \text{(A16)}$$

First Derivatives – Reactive power

$$\frac{\partial G^{Q_c}}{\partial U_c} = -2 \cdot U_{c,i} \cdot B_{tc} + U_{s,i} \cdot [G_{tc} \cdot \sin(\theta_{s,i} - \theta_{c,i}) + B_{tc} \cdot \cos(\theta_{s,i} - \theta_{c,i})] \quad \text{(A17)}$$

$$\frac{\partial G^{Q_c}}{\partial U_s} = U_{c,i} \cdot [G_{tc} \cdot \sin(\theta_{s,i} - \theta_{c,i}) + B_{tc} \cdot \cos(\theta_{s,i} - \theta_{c,i})] \quad \text{(A18)}$$

$$\frac{\partial G^{Q_c}}{\partial \theta_c} = U_{c,i} \cdot U_{s,i} \cdot [-G_{tc} \cdot \cos(\theta_{s,i} - \theta_{c,i}) + B_{tc} \cdot \sin(\theta_{s,i} - \theta_{c,i})] \quad \text{(A19)}$$

$$\frac{\partial G^{Q_c}}{\partial \theta_s} = U_{c,i} \cdot U_{s,i} \cdot [G_{tc} \cdot \cos(\theta_{s,i} - \theta_{c,i}) - B_{tc} \cdot \sin(\theta_{s,i} - \theta_{c,i})] \quad \text{(A20)}$$

$$\frac{\partial G^{Q_c}}{\partial P_c} = 0 \quad \text{(A21)}$$

$$\frac{\partial G^{Q_c}}{\partial Q_c} = -1 \quad \text{(A22)}$$

Second Derivatives – Active power

$$\frac{\partial G^{P_c}}{\partial U_c^2} = 2 \cdot G_{tc} \quad \text{(A23)}$$

$$\frac{\partial G^{P_c}}{\partial U_c \partial U_s} = -\left(G_{tc} \cdot \cos(\theta_{s,i} - \theta_{c,i}) - B_{tc} \cdot \sin(\theta_{s,i} - \theta_{c,i})\right) \quad \text{(A24)}$$

$$\frac{\partial G^{P_c}}{\partial U_c \partial \theta_c} = -U_{s,i} \cdot \left(G_{tc} \cdot \sin(\theta_{s,i} - \theta_{c,i}) + B_{tc} \cdot \cos(\theta_{s,i} - \theta_{c,i})\right) \quad \text{(A25)}$$

$$\frac{\partial G^{P_c}}{\partial U_c \partial \theta_s} = -U_{s,i} \cdot \left(-G_{tc} \cdot \sin\left(\theta_{s,i} - \theta_{c,i}\right) - B_{tc} \cdot \cos\left(\theta_{s,i} - \theta_{c,i}\right)\right) \quad \text{(A26)}$$

$$\frac{\partial G^{P_c}}{\partial U_s \partial U_c} = -\left(G_{tc} \cdot \cos\left(\theta_{s,i} - \theta_{c,i}\right) - B_{tc} \cdot \sin\left(\theta_{s,i} - \theta_{c,i}\right)\right) \quad \text{(A27)}$$

$$\frac{\partial G^{P_c}}{\partial U_s^2} = 0 \quad \text{(A28)}$$

$$\frac{\partial G^{P_c}}{\partial U_s \partial \theta_c} = -U_{c,i} \cdot \left(G_{tc} \cdot \sin\left(\theta_{s,i} - \theta_{c,i}\right) + B_{tc} \cdot \cos\left(\theta_{s,i} - \theta_{c,i}\right)\right) \quad \text{(A29)}$$

$$\frac{\partial G^{P_c}}{\partial U_s \partial \theta_s} = -U_{c,i} \cdot \left(-G_{tc} \cdot \sin\left(\theta_{s,i} - \theta_{c,i}\right) - B_{tc} \cdot \cos\left(\theta_{s,i} - \theta_{c,i}\right)\right) \quad \text{(A30)}$$

$$\frac{\partial G^{P_c}}{\partial \theta_c \partial U_c} = -U_{s,i} \cdot \left(G_{tc} \cdot \sin\left(\theta_{s,i} - \theta_{c,i}\right) + B_{tc} \cdot \cos\left(\theta_{s,i} - \theta_{c,i}\right)\right) \quad \text{(A31)}$$

$$\frac{\partial G^{P_c}}{\partial \theta_c \partial U_s} = -U_{c,i} \cdot \left(G_{tc} \cdot \sin\left(\theta_{s,i} - \theta_{c,i}\right) + B_{tc} \cdot \cos\left(\theta_{s,i} - \theta_{c,i}\right)\right) \quad \text{(A32)}$$

$$\frac{\partial G^{P_c}}{\partial \theta_c^2} = -U_c \cdot U_{s,i} \cdot \left(-G_{tc} \cdot \cos\left(\theta_{s,i} - \theta_{c,i}\right) + B_{tc} \cdot \sin\left(\theta_{s,i} - \theta_{c,i}\right)\right) \quad \text{(A33)}$$

$$\frac{\partial G^{P_c}}{\partial \theta_c \partial \theta_s} = -U_{c,i} \cdot U_{s,i} \cdot \left(G_{tc} \cdot \cos\left(\theta_{s,i} - \theta_{c,i}\right) - B_{tc} \cdot \sin\left(\theta_{s,i} - \theta_{c,i}\right)\right) \quad \text{(A34)}$$

$$\frac{\partial G^{P_c}}{\partial \theta_s \partial U_c} = -U_{s,i} \cdot \left(-G_{tc} \cdot \sin\left(\theta_{s,i} - \theta_{c,i}\right) - B_{tc} \cdot \cos\left(\theta_{s,i} - \theta_{c,i}\right)\right) \quad \text{(A35)}$$

$$\frac{\partial G^{P_c}}{\partial \theta_s \partial U_s} = -U_{c,i} \cdot \left(-G_{tc} \cdot \sin\left(\theta_{s,i} - \theta_{c,i}\right) - B_{tc} \cdot \cos\left(\theta_{s,i} - \theta_{c,i}\right)\right) \quad \text{(A36)}$$

$$\frac{\partial G^{P_c}}{\partial \theta_s \partial \theta_c} = -U_{c,i} \cdot U_{s,i} \cdot \left(G_{tc} \cdot \cos\left(\theta_{s,i} - \theta_{c,i}\right) - B_{tc} \cdot \sin\left(\theta_{s,i} - \theta_{c,i}\right)\right) \quad \text{(A37)}$$

$$\frac{\partial G^{P_c}}{\partial \theta_s^2} = -U_{c,i} \cdot U_{s,i} \cdot \left(-G_{tc} \cdot \cos\left(\theta_{s,i} - \theta_{c,i}\right) + B_{tc} \cdot \sin\left(\theta_{s,i} - \theta_{c,i}\right)\right) \quad \text{(A38)}$$

Second Derivatives – Reactive power

$$\frac{\partial G^{Q_c}}{\partial U_c^2} = -2 \cdot B_{tc} \quad \text{(A39)}$$

$$\frac{\partial G^{Q_c}}{\partial U_c \partial U_s} = G_{tc} \cdot \sin\left(\theta_{s,i} - \theta_{c,i}\right) + B_{tc} \cdot \cos\left(\theta_{s,i} - \theta_{c,i}\right) \quad \text{(A40)}$$

$$\frac{\partial G^{Q_c}}{\partial U_c \partial \theta_c} = U_{s,i} \cdot (-G_{tc} \cdot \cos(\theta_{s,i} - \theta_{c,i}) + B_{tc} \cdot \sin(\theta_{s,i} - \theta_{c,i})) \quad \text{(A41)}$$

$$\frac{\partial G^{Q_c}}{\partial U_c \partial \theta_s} = U_{s,i} \cdot (G_{tc} \cdot \cos(\theta_{s,i} - \theta_{c,i}) - B_{tc} \cdot \sin(\theta_{s,i} - \theta_{c,i})) \quad \text{(A42)}$$

$$\frac{\partial G^{Q_c}}{\partial U_s \partial U_c} = G_{tc} \cdot \sin(\theta_{s,i} - \theta_{c,i}) + B_{tc} \cdot \cos(\theta_{s,i} - \theta_{c,i}) \quad \text{(A43)}$$

$$\frac{\partial G^{Q_c}}{\partial U_s^2} = 0 \quad \text{(A44)}$$

$$\frac{\partial G^{Q_c}}{\partial U_s \partial \theta_c} = U_{c,i} \cdot (-G_{tc} \cdot \cos(\theta_{s,i} - \theta_{c,i}) + B_{tc} \cdot \sin(\theta_{s,i} - \theta_{c,i})) \quad \text{(A45)}$$

$$\frac{\partial G^{Q_c}}{\partial U_s \partial \theta_s} = U_{c,i} \cdot (G_{tc} \cdot \cos(\theta_{s,i} - \theta_{c,i}) - B_{tc} \cdot \sin(\theta_{s,i} - \theta_{c,i})) \quad \text{(A46)}$$

$$\frac{\partial G^{Q_c}}{\partial \theta_c \partial U_c} = U_{s,i} \cdot (-G_{tc} \cdot \cos(\theta_{s,i} - \theta_{c,i}) + B_{tc} \cdot \sin(\theta_{s,i} - \theta_{c,i})) \quad \text{(A47)}$$

$$\frac{\partial G^{Q_c}}{\partial \theta_c \partial U_s} = U_{c,i} \cdot (-G_{tc} \cdot \cos(\theta_{s,i} - \theta_{c,i}) + B_{tc} \cdot \sin(\theta_{s,i} - \theta_{c,i})) \quad \text{(A48)}$$

$$\frac{\partial G^{Q_c}}{\partial \theta_c^2} = U_{c,i} \cdot U_{s,i} \cdot (-G_{tc} \cdot \sin(\theta_{s,i} - \theta_{c,i}) - B_{tc} \cdot \cos(\theta_{s,i} - \theta_{c,i})) \quad \text{(A49)}$$

$$\frac{\partial G^{Q_c}}{\partial \theta_c \partial \theta_s} = U_{c,i} \cdot U_{s,i} \cdot (G_{tc} \cdot \sin(\theta_{s,i} - \theta_{c,i}) + B_{tc} \cdot \cos(\theta_{s,i} - \theta_{c,i})) \quad \text{(A50)}$$

$$\frac{\partial G^{Q_c}}{\partial \theta_s \partial U_c} = U_{s,i} \cdot (G_{tc} \cdot \cos(\theta_{s,i} - \theta_{c,i}) - B_{tc} \cdot \sin(\theta_{s,i} - \theta_{c,i})) \quad \text{(A51)}$$

$$\frac{\partial G^{Q_c}}{\partial \theta_s \partial U_s} = U_{c,i} \cdot (G_{tc} \cdot \cos(\theta_{s,i} - \theta_{c,i}) - B_{tc} \cdot \sin(\theta_{s,i} - \theta_{c,i})) \quad \text{(A52)}$$

$$\frac{\partial G^{Q_c}}{\partial \theta_s \partial \theta_c} = U_{c,i} \cdot U_{s,i} \cdot (G_{tc} \cdot \sin(\theta_{s,i} - \theta_{c,i}) + B_{tc} \cdot \cos(\theta_{s,i} - \theta_{c,i})) \quad \text{(A53)}$$

$$\frac{\partial G^{Q_c}}{\partial \theta_s^2} = U_{c,i} \cdot U_{s,i} \cdot (-G_{tc} \cdot \sin(\theta_{s,i} - \theta_{c,i}) - B_{tc} \cdot \cos(\theta_{s,i} - \theta_{c,i})) \quad \text{(A54)}$$

Appendix 2: Input data matrices for the test system

In this appendix, all the input data for the test system are tabulated, organized in different matrices: bus matrix (divided into two parts), generator matrix, AC branch matrix (divided into two parts), VSC converters matrix and HVDC branch matrix; as presented in the MatPower interface. The input data tables are shown for the case of the test system in stage 3, which includes the total number of converters and the total number of HVDC lines. It should be noted that the boxes containing variable data are shown in blue.

Appendix 2.1: Bus input data matrix

Table A2.1: Bus input data matrix for the test system: part 1.

Bus Data I										
bus_i	**type**	**Pd (MW)**	**Qd (Mvar)**	**Area**	**Vm (pu)**	**Va (°)**	**baseV (kV)**	**Zone**	**Vmax (pu)**	**Vmin (pu)**
1	3	0	0	1	1.00	0.00	380	1	1.10	0.90
2	1	-1500	-100	1	1.00	0.00	380	1	1.10	0.90
3	2	0	0	1	1.00	0.00	380	1	1.10	0.90
4	2	0	0	1	1.00	0.00	380	1	1.10	0.90
5	1	-1200	-100	1	1.00	0.00	380	1	1.10	0.90
6	1	191	76	1	1.00	0.00	380	1	1.10	0.90
7	2	0	0	1	1.00	0.00	380	1	1.10	0.90
8	1	287	73	1	1.00	0.00	380	1	1.10	0.90
9	1	186	74	1	1.00	0.00	380	1	1.10	0.90
10	2	0	0	1	1.00	0.00	380	1	1.10	0.90
11	1	271	55	1	1.00	0.00	380	1	1.10	0.90
12	1	171	87	1	1.00	0.00	380	1	1.10	0.90
13	2	0	0	1	1.00	0.00	380	1	1.10	0.90
14	1	199	60	1	1.00	0.00	380	1	1.10	0.90
15	1	113	52.5	1	1.00	0.00	380	1	1.10	0.90
16	1	38	7	1	1.00	0.00	380	1	1.10	0.90
17	1	275	106	1	1.00	0.00	380	1	1.10	0.90
18	2	0	0	1	1.00	0.00	380	1	1.10	0.90
19	1	165	46	1	1.00	0.00	380	1	1.10	0.90
20	1	178	82.5	1	1.00	0.00	380	1	1.10	0.90
21	1	0	0	1	1.00	0.00	380	1	1.10	0.90
22	1	30	7	1	1.00	0.00	380	1	1.10	0.90
23	2	0	0	1	1.00	0.00	380	1	1.10	0.90
24	1	32	7	1	1.00	0.00	380	1	1.10	0.90
25	2	0	0	1	1.00	0.00	380	1	1.10	0.90
26	1	395	89	2	1.00	0.00	380	1	1.10	0.90
27	2	0	0	2	1.00	0.00	380	1	1.10	0.90
28	1	665	99	2	1.00	0.00	380	1	1.10	0.90
29	2	0	0	2	1.00	0.00	380	1	1.10	0.90
30	1	266	100	2	1.00	0.00	380	1	1.10	0.90
31	1	845	119	2	1.00	0.00	380	1	1.10	0.90
32	1	332	137	2	1.00	0.00	380	1	1.10	0.90

Table A2.2: Bus input data matrix for the test system: part 2.

Bus Data II										
bus_i	**type**	**Pd (MW)**	**Qd (Mvar)**	**Area**	**Vm (pu)**	**Va (°)**	**baseV (kV)**	**Zone**	**Vmax (pu)**	**Vmin (pu)**
33	2	0	0	2	1.00	0.00	380	1	1.10	0.90
34	1	540	158	2	1.00	0.00	380	1	1.10	0.90
35	1	460	97	2	1.00	0.00	380	1	1.10	0.90
36	2	0	0	2	1.00	0.00	380	1	1.10	0.90
37	1	451	190	2	1.00	0.00	380	1	1.10	0.90
38	1	150	0	2	1.00	0.00	380	1	1.10	0.90
39	1	629	87	2	1.00	0.00	380	1	1.10	0.90
40	2	0	0	2	1.00	0.00	380	1	1.10	0.90
41	2	0	0	2	1.00	0.00	380	1	1.10	0.90
42	1	859	180	2	1.00	0.00	380	1	1.10	0.90
43	2	0	0	2	1.00	0.00	380	1	1.10	0.90
44	1	474	92	2	1.00	0.00	380	1	1.10	0.90
45	1	668	109	2	1.00	0.00	380	1	1.10	0.90
46	1	614	95	2	1.00	0.00	380	1	1.10	0.90
47	1	81	-50	2	1.00	0.00	380	1	1.10	0.90
48	2	0	0	2	1.00	0.00	380	1	1.10	0.90
49	1	0	0	2	1.00	0.00	380	1	1.10	0.90
50	2	0	0	2	1.00	0.00	380	1	1.10	0.90
51	1	430	123	2	1.00	0.00	380	1	1.10	0.90
52	1	309	102	3	1.00	0.00	380	1	1.10	0.90
53	1	100	30	3	1.00	0.00	380	1	1.10	0.90
54	2	0	0	3	1.00	0.00	380	1	1.10	0.90
55	1	303	110	3	1.00	0.00	380	1	1.10	0.90
56	2	0	0	3	1.00	0.00	380	1	1.10	0.90
57	2	0	0	3	1.00	0.00	380	1	1.10	0.90
58	1	324	157	3	1.00	0.00	380	1	1.10	0.90
59	2	0	0	3	1.00	0.00	380	1	1.10	0.90
60	1	115	42	3	1.00	0.00	380	1	1.10	0.90
61	1	187	75	3	1.00	0.00	380	1	1.10	0.90
62	1	319	95	3	1.00	0.00	380	1	1.10	0.90
63	2	0	0	3	1.00	0.00	380	1	1.10	0.90
64	2	0	0	3	1.00	0.00	380	1	1.10	0.90
65	1	315	97	3	1.00	0.00	380	1	1.10	0.90
66	2	0	0	3	1.00	0.00	380	1	1.10	0.90

Appendix 2.2: Generators input data matrix

Table A2.3: Generators input data matrix for the test system.

Generators Data									
bus	**Pg (MW)**	**Qg (Mvar)**	**Qmax (Mvar)**	**Qmin (Mvar)**	**Vg (pu)**	**mBase**	**status**	**Pmax (MW)**	**Pmin (MW)**
1	800.793733	22.805901	1000	-500	1.052632	1500	1	1000	400
4	523.00	141.048321	350	-350	1.052632	1500	1	560	220
10	436.00	106.545757	350	-350	1.052632	1500	1	560	220
13	541.00	118.272949	300	-300	1.052632	1500	1	630	250
18	681.00	-31.607769	400	-400	1.026316	1500	1	720	300
25	469.00	60.146949	250	-250	1.039474	1500	1	560	220
29	500.00	100.195450	350	-350	1.026316	1500	1	630	250
33	496.00	305.933255	500	-500	1.026316	1500	1	850	350
36	512.00	248.825328	400	-400	1.026316	1500	1	720	300
41	350.00	230.478296	450	-450	1.039474	1500	1	850	350
43	574.00	233.526045	500	-250	1.026316	1500	1	720	220
50	581.00	149.886082	400	-400	1.039474	1500	1	720	300
56	496.00	56.359801	250	-250	1.039474	1500	1	560	220
59	431.00	205.939667	350	-350	1.044737	1500	1	720	300
63	488.00	152.216856	250	-300	1.044737	1500	1	520	250
64	300.00	61.043416	250	-400	1.047368	1500	1	560	250
66	537.00	144.008771	300	-400	1.044737	1500	1	630	250

Appendix 2.3: AC branches input data matrix

Table A2.4: AC branches input data matrix for the test system: part 1.

Branch Data I							
fbus	**tbus**	**r (pu)**	**x (pu)**	**b (pu)**	**rateA**	**rateB**	**rateC**
1	5	0.002078	0.017313019	0	1000	0	0
1	7	0.002078	0.017313019	0	1000	0	0
1	8	0.002078	0.017313019	0	1000	0	0
1	14	0.002078	0.017313019	0	1000	0	0
2	3	0.002078	0.017313019	0	1000	0	0
2	9	0.002078	0.017313019	0	1000	0	0
3	4	0.002078	0.017313019	0	1000	0	0
2	12	0.002078	0.017313019	0	1000	0	0
3	10	0.002078	0.017313019	0	1000	0	0
3	12	0.002078	0.017313019	0	1000	0	0
3	9	0.002078	0.017313019	0	1000	0	0
4	14	0.002078	0.017313019	0	1000	0	0
4	19	0.002078	0.017313019	0	1000	0	0
5	6	0.002078	0.017313019	0	1000	0	0
5	7	0.002078	0.017313019	0	1000	0	0
5	8	0.002078	0.017313019	0	1000	0	0
6	7	0.002078	0.017313019	0	1000	0	0
7	15	0.002078	0.017313019	0	1000	0	0
7	16	0.002078	0.017313019	0	1000	0	0
8	9	0.002078	0.017313019	0	1000	0	0
10	11	0.002078	0.017313019	0	1000	0	0
10	22	0.002078	0.017313019	0	1000	0	0
11	12	0.002078	0.017313019	0	1000	0	0
11	13	0.002078	0.017313019	0	1000	0	0
12	13	0.002078	0.017313019	0	1000	0	0
13	53	0.002078	0.017313019	0	1000	0	0
14	15	0.002078	0.017313019	0	1000	0	0
14	18	0.002078	0.017313019	0	1000	0	0
16	17	0.002078	0.017313019	0	1000	0	0
16	18	0.002078	0.017313019	0	1000	0	0
17	24	0.002078	0.017313019	0	1000	0	0
18	20	0.002078	0.017313019	0	1000	0	0
18	24	0.002078	0.017313019	0	1000	0	0
19	20	0.002078	0.017313019	0	1000	0	0
19	23	0.002078	0.017313019	0	1000	0	0
20	21	0.002078	0.017313019	0	1000	0	0
21	22	0.002078	0.017313019	0	1000	0	0
21	23	0.002078	0.017313019	0	1000	0	0
21	25	0.002078	0.017313019	0	1000	0	0
22	25	0.002078	0.017313019	0	1000	0	0
22	56	0.002078	0.017313019	0	1000	0	0
24	49	0.002078	0.017313019	0	1000	0	0
25	43	0.002078	0.017313019	0	1000	0	0
26	27	0.002078	0.017313019	0	1000	0	0
26	30	0.002078	0.017313019	0	1000	0	0
26	31	0.002078	0.017313019	0	1000	0	0
26	40	0.002078	0.017313019	0	1000	0	0
27	28	0.002078	0.017313019	0	1000	0	0
27	31	0.002078	0.017313019	0	1000	0	0
28	35	0.002078	0.017313019	0	1000	0	0
28	37	0.002078	0.017313019	0	1000	0	0

Table A2.5: AC branches input data matrix for the test system: part 2.

Branch Data II							
fbus	**tbus**	**r (pu)**	**x (pu)**	**b (pu)**	**rateA**	**rateB**	**rateC**
29	35	0.002078	0.017313019	0	1000	0	0
29	39	0.002078	0.017313019	0	1000	0	0
29	44	0.002078	0.017313019	0	1000	0	0
30	31	0.002078	0.017313019	0	1000	0	0
30	32	0.002078	0.017313019	0	1000	0	0
32	40	0.002078	0.017313019	0	1000	0	0
33	34	0.002078	0.017313019	0	1000	0	0
33	35	0.002078	0.017313019	0	1000	0	0
33	51	0.002078	0.017313019	0	1000	0	0
34	51	0.002078	0.017313019	0	1000	0	0
35	36	0.002078	0.017313019	0	1000	0	0
35	47	0.002078	0.017313019	0	1000	0	0
36	37	0.002078	0.017313019	0	1000	0	0
36	38	0.002078	0.017313019	0	1000	0	0
37	38	0.002078	0.017313019	0	1000	0	0
39	40	0.002078	0.017313019	0	1000	0	0
39	43	0.002078	0.017313019	0	1000	0	0
40	41	0.002078	0.017313019	0	1000	0	0
41	42	0.002078	0.017313019	0	1000	0	0
42	43	0.002078	0.017313019	0	1000	0	0
42	49	0.002078	0.017313019	0	1000	0	0
43	44	0.002078	0.017313019	0	1000	0	0
43	49	0.002078	0.017313019	0	1000	0	0
44	45	0.002078	0.017313019	0	1000	0	0
44	48	0.002078	0.017313019	0	1000	0	0
45	46	0.002078	0.017313019	0	1000	0	0
45	50	0.002078	0.017313019	0	1000	0	0
47	48	0.002078	0.017313019	0	1000	0	0
46	48	0.002078	0.017313019	0	1000	0	0
47	50	0.002078	0.017313019	0	1000	0	0
47	51	0.002078	0.017313019	0	1000	0	0
47	59	0.002078	0.017313019	0	1000	0	0
52	53	0.002078	0.017313019	0	1000	0	0
52	54	0.002078	0.017313019	0	1000	0	0
52	64	0.002078	0.017313019	0	1000	0	0
54	65	0.002078	0.017313019	0	1000	0	0
54	66	0.002078	0.017313019	0	1000	0	0
55	57	0.002078	0.017313019	0	1000	0	0
55	63	0.002078	0.017313019	0	1000	0	0
56	58	0.002078	0.017313019	0	1000	0	0
56	59	0.002078	0.017313019	0	1000	0	0
57	58	0.002078	0.017313019	0	1000	0	0
57	63	0.002078	0.017313019	0	1000	0	0
58	60	0.002078	0.017313019	0	1000	0	0
58	61	0.002078	0.017313019	0	1000	0	0
59	60	0.002078	0.017313019	0	1000	0	0
61	62	0.002078	0.017313019	0	1000	0	0
62	63	0.002078	0.017313019	0	1000	0	0
62	66	0.002078	0.017313019	0	1000	0	0
65	66	0.002078	0.017313019	0	1000	0	0
66	64	0.002078	0.017313019	0	1000	0	0

Appendix 2.4: VSC converters input data matrix

Table A2.6: VSC converters input data matrix for the test system.

VSC Converters Data						
Nconv	AC bus	Ps (MW)	Qs (Mvar)	Psmax (MW)	Qsmax (Mvar)	Vc (pu)
1	3	-553.725074	113.300554	2000	1000	1.00
2	7	-553.509400	355.128590	2000	1000	1.00
3	23	-603.338373	255.599579	2000	1000	1.00
4	27	996.380364	558.336834	2000	1000	1.00
5	40	996.499337	272.949505	2000	1000	1.00
6	48	996.612471	445.632712	2000	1000	1.00
7	54	469.404427	128.794544	2000	1000	1.00
8	57	-553.051856	291.252835	2000	1000	1.00
Angc (°)	Vsmax (pu)	Vsmin (pu)	Vdc (pu)	dcBase (kV)	Vdcmax (pu)	Vdcmin (pu)
0.00	1.10	0.90	1.00	500	1.10	0.90
0.00	1.10	0.90	1.00	500	1.10	0.90
0.00	1.10	0.90	1.00	500	1.10	0.90
0.00	1.10	0.90	1.00	500	1.10	0.90
0.00	1.10	0.90	1.00	500	1.10	0.90
0.00	1.10	0.90	1.00	500	1.10	0.90
0.00	1.10	0.90	1.00	500	1.10	0.90
0.00	1.10	0.90	1.00	500	1.10	0.90

Appendix 2.5: HVDC branches input data matrix

Table A2.7: HVDC branches input data matrix for the test system.

HVDC Branch Data			
fromConv	**toConv**	**r (pu)**	**ImaxDC (A)**
2	5	3.00E-04	3500
1	3	3.00E-04	3500
3	6	3.00E-04	3500
7	8	3.00E-04	3500
1	2	3.00E-04	3500
5	4	3.00E-04	3500
6	4	3.00E-04	3500
7	3	3.00E-04	3500
3	5	3.00E-04	3500
8	6	3.00E-04	3500

Bibliography

[1] European Comission, *Climate Action: 2030 climate & energy framework.* [Online]. Available: https://ec.europa.eu/clima/eu-action/climate-strategies-targets/2030-climate-energy-framework_en (accessed: January 2022).

[2] D. Van Hertem, O. Gomis-Bellmunt, J. Liang, *HVDC Grids: For Offshore and Supergrid of the Future,* 1st ed.: John Wiley & Sons, Inc., 2016.

[3] J. Cao, J. Y. Cai, *EPRI HVDC & FACTS Conference: HVDC in China.* [Online]. Available: www.dsius.com/cet/HVDCinChina_EPRI2013_HVDC.pdf (accessed: January 2022).

[4] Ray D. Zimmerman, Carlos E. Murillo-Sánchez, *MatPower - User's Manual for Version 7.0,* 7th ed., 2019.

[5] C. Garcia-Aguilar, "Descripción y estudio de los enlaces HVDC en los sistemas eléctricos," Bachelor Thesis, Escola Tècnica Superior d'Enginyeria Industrial de Barcelona, Universitat Politècnica de Catalunya, Barcelona (Spain), 2020.

[6] A. Silos-Sanchez, "Wind Generation for Energy Engineers - HVDC Transmission Lines and Off-shore Wind Farms," Barcelona (Spain), April 2021.

[7] Megger Group (K. Wilson), *Transmisión alta tensión en 1904.* [Online]. Available: https://es.megger.com/electrical-tester-online/julio-2021/transmision-alta-tension-cc-%C2%A1en-1904! (accessed: January 2022).

[8] W. Litzenberger, "A Short History of the Pacific HVDC Intertie," in *2006 IEEE PES Power Systems Conference and Exposition*, Atlanta, Georgia, USA, 2006, pp. 24–27.

[9] V. Lieste, E. Blocher (Siemens), *Cahora Bassa - Südafrika HVDC.* [Online]. Available: https://new.siemens.com/de/de/unternehmen/konzern/geschichte/stories/siemens-versorgt-suedafrika-mit-strom.html (accessed: January 2022).

[10] Th. Westerweller (Siemens AG), J. J. Price (England National Grid), *Basslink HVDC Interconnector - System Design Considerations.* [Online]. Available: https://www.ptd.siemens.de/IEE_HVDC_0306.pdf (accessed: January 2022).

[11] D. Loume, M. Nguyen, A. Bertinato, B. Raison, Ed., *DC cable modelling and High Voltage Direct Current grid grounding system*, 2015.

[12] M. Schwenke, "Optimal Supply of Heat and Electrical Energy in District Networks using Multi-Period AC Optimal Power Flow Algorithms," Master Thesis, Fachgebiet Elektrische Energieversorgung unter Einsatz Erneuerbarer Energien, TU Darmstadt, Darmstadt (Germany), 2021.

[13] R. Benato, “A Basic AC Power Flow based on The Bus Admittance Matrix incorporating Loads and Generators including Slack Bus,” *IEEE Trans. Power Syst.*, p. 1, 2021, doi: 10.1109/TPWRS.2021.3104097.

[14] J. Cao, W. Du, H. F. Wang, and S. Q. Bu, “Minimization of Transmission Loss in Meshed AC/DC Grids With VSC-MTDC Networks,” *IEEE Trans. Power Syst.*, vol. 28, no. 3, pp. 3047–3055, 2013, doi: 10.1109/TPWRS.2013.2241086.

[15] A. Sumper, J. J. Mesas, *Sistemas Eléctricos de Potencia*. Barcelona (Spain): UPC-BarcelonaTech, 2019.

[16] J. Rimez, “Optimal Operation of Hybrid AC/DC Meshed Grids,” Doctoral Thesis, Faculty of Engineering Science, KU Leuven, Leuven (Belgium), 2014.

[17] R. Wiget and G. Andersson, “Optimal power flow for combined AC and multi-terminal HVDC grids based on VSC converters,” in *2012 IEEE Power and Energy Society General Meeting*, San Diego, CA, 2012, pp. 1–8.

[18] X.-P. Zhang, “Multiterminal Voltage-Sourced Converter-Based HVDC Models for Power Flow Analysis,” *IEEE Trans. Power Syst.*, vol. 19, no. 4, pp. 1877–1884, 2004, doi: 10.1109/TPWRS.2004.836250.

[19] L. Zhang *et al.,* “Modeling, control, and protection of modular multilevel converter-based multi-terminal HVDC systems: A review,” *CSEE JPES*, vol. 3, no. 4, pp. 340–352, 2017, doi: 10.17775/CSEEJPES.2017.00440.

[20] K. Rouzbehi, A. Miranian, J. I. Candela, A. Luna, and P. Rodriguez, “A Generalized Voltage Droop Strategy for Control of Multiterminal DC Grids,” *IEEE Trans. on Ind. Applicat.*, vol. 51, no. 1, pp. 607–618, 2015, doi: 10.1109/TIA.2014.2332814.

[21] J. Tello Maita, A. Marulanda Guerra, Ed., *Interior Point Methods in Optimal Power Flow solvers comparison using Matlab*. Maracaibo (Venezuela), 2013.

[22] Ray D. Zimmerman, *AC Power Flows, Generalized OPF Costs and their Derivatives using Complex Matrix Notation: Matpower Technical Note 2*. Revision 5, 2018.

[23] Ray D. Zimmerman, *Addendum to AC Power Flows and their Addendum to AC Power Flows and their Addendum to AC Power Flows and their Derivatives using Complex Matrix Notation: Nodal Current Balance: Matpower Technical Note 3*, 2018.

[24] J. Beerten, S. Cole, and R. Belmans, “Generalized Steady-State VSC MTDC Model for Sequential AC/DC Power Flow Algorithms,” *IEEE Trans. Power Syst.*, vol. 27, no. 2, pp. 821–829, 2012, doi: 10.1109/TPWRS.2011.2177867.

[25] P. Lundberg (ABB Group), *HVDC Light: Power from shore.* [Online]. Available: https://new.abb.com/docs/librariesprovider46/pw2016/seminars/r607-en-abb_hvdc_light_power_from_shore.pdf?sfvrsn=2 (accessed: December 2021).

[26] A. Cabrera-Tobar, E. Bullich-Massagué, M. Aragüés-Peñalba, and O. Gomis-Bellmunt, Eds., *Reactive power capability analysis of a photovoltaic generator for large scale power plants*. Barcelona (Spain): IET, 2016.

[27] F. Sass, T. Sennewald, A. Marten, and D. Westermann, “Mixed AC high-voltage direct current benchmark test system for security constrained optimal power flow calculation,” *IET Generation, Transmission & Distribution*, vol. 11, no. 2, pp. 447–455, 2017, doi: 10.1049/iet-gtd.2016.0993.

[28] J. Beerten, *MatACDC 1.0 - User's Manual*. Leuven (Belgium), 2012.